Studies on Photocatalytic Hydrogen Evolution Reaction System Focused on Surface Passivating Ligands for the CdSe Quantum Dot

（CdSe 量子ドットの表面保護配位子に着目した水素発生反応系の研究）

Kana Sato (Sawaguchi)

Graduate School of Chemical Sciences and Engineering
Hokkaido University
2017

Contents

Chapter 1

General Introduction

1-1 Solar water splitting and photocatalyst[1]

In recent years, global energy issue has grown a serious problem because of large consumption of fossil fuels. To solve this global issue, developments of alternative energies to fossil fuels have been extensively researched. Especially, solar energy has been expected to be one of the most promising energy resources, because it is clean and inexhaustible energy. A photocatalytic water splitting reaction driven by solar light energy, so called "artificial photosynthesis", have been extensively studied to apply this reaction to industrial application because it can convert the solar energy to useful and clean chemical energies as hydrogen (H_2) and oxygen (O_2) without any environmental pollutants like carbon dioxide.

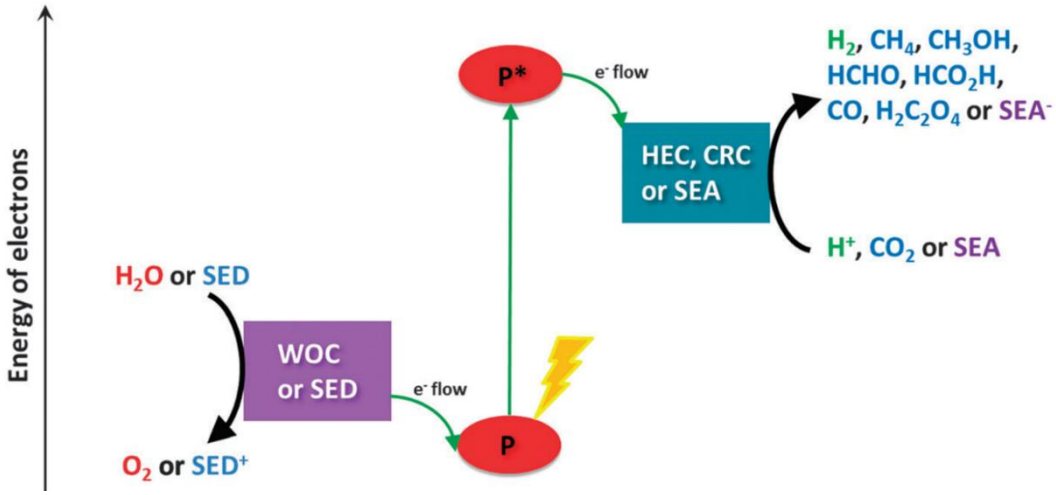

Scheme 1-1. Schematic diagram of artificial photosynthesis driven by photosensitizer (P), water oxidation catalyst (WOC), sacrificial electron donor (SED), H_2 evolution catalyst (HEC), carbon reduction catalyst (CRC) and sacrificial electron acceptor (SEA).[1b]

There are three essential functions in the photocatalysts for water splitting reaction as shown in Scheme 1-1. The first is photo-redox sensitizing (PS) ability to form charge-separated state by absorption of solar light. The second is a catalytic ability to reduce protons (RC: reduction catalyst) to form H_2 after receiving the excited electrons from PS. The third is also a catalytic ability to oxidize water molecule (OC: oxidation catalyst) to form O_2 after receiving the holes from PS. These essential functions clearly indicate that developments not only highly active catalysts for both H_2 and O_2

generations, but also the photosensitizer to absorb solar light and then transfer the excited electron and hole to the catalysts are highly required. Especially, the development of photosensitizing ability to absorb solar light and then separate effectively the photo-generated electron-hole pair (exciton) is a critical issue to improve the energy conversion efficiency of photocatalyst from solar light to chemical energy.

1-1-1 Photocatalytic H_2 Evolution Reaction

Extensive studies of photocatalytic water splitting was triggered by Honda and Fujishima's report on TiO_2 photonanode in 1972.[2] In plants, many metal complexes play important roles in natural photosynthesis especially in the water oxidation by Mn_4Ca cluster as shown in Figure 1-1). Thus, the study of photocatalytic water splitting using metal complex catalysts have been done energetically from a viewpoint of mimicking the natural photosynthesis. Metal complex have the advantage for molecular design, because of the wide variety of metal ions and structural diversity of organic ligands. Therefore, metal complex system has been expected not only to create highly active catalysts but also to clarify the detail of reaction mechanism in natural photosynthesis.[3]

On the other hand, semiconductor materials including TiO_2 have also been studied to apply photocatalytic water splitting reaction because of the superior photodurability compared to the metal complex system.[4]

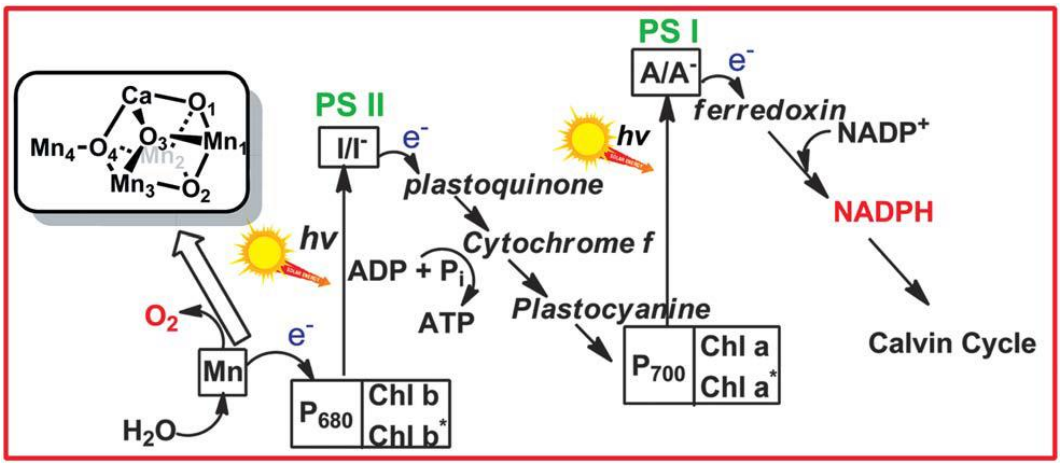

Figure 1-1. Two-step photoinduced-electron transfer reaction in natural photosynthesis (so called "Z scheme").[4]

In case of photocatalytic water splitting reaction using metal complex, there are many report about half reaction (only H_2 evolution reaction or water oxidation reaction) in homogeneous system. In H_2 evolution reaction, metal complexes using Pt,[5] Pd,[6] Co,[7] Rh,[8] Fe[9], Ni[10] ions have been developed as the active H_2 evolution catalyst. However, most of the reaction intermediates generated in the catalytic process (one electron-reduced or -oxidized species), are not stable enough to wait and receive several electrons. Thus, the decomposition of metal complex catalyst could be one of the critical issues for practical application. This problem is more critical in the oxygen evolution (water oxidation) reaction. Although metal complexes using Ru,[11] Mn,[12] or Co[13] ions have been developed as the oxygen evolution catalysts, four-electron transfer reaction from oxidation catalyst to photosensitizer is necessary to evolve dioxygen. In addition, it is still challenging issue to combine these two catalysts to achieve solar water splitting.

In the researches for photocatalytic water splitting based on semiconductor materials, various semiconductors, metal oxides, nitrides, and sulfides have been studied so far.[5] Especially, metal oxides including TiO_2 have attracted much attention because of their high stability and catalytic activity. In the metal oxides, the valence band (VB) is generally formed by the 2p orbitals of oxygen atoms and locates at more positive potential than 3.0 V (vs. NHE), which enables them to oxidize water molecules to evolve dioxygen. Since the conduction band (CB) is formed by the d and/or s orbitals of the metal

ion, the position of CB can be modified by changing the metal ion. In the case of metal oxides which have negative potential of CB suitable for H_2 evolution reaction (less than 0 V vs NHE), the corresponding VB tends to locate at deeply positive position. Thus, the band gap became larger than over 3 eV, resulting in the limitation of light adsorption ability only in UV region. Some metal oxides can absorb visible light (e.g. WO_3 and In_2O), but these oxides do not have enough potential to drive H_2 evolution reaction because of more positive potential of CB than 0 V vs NHE. Therefore, most of photocatalytic water splitting reactions using metal oxides are driven only UV region. To address this issue, several methods to develop visible-light-driven water splitting photocatalysts have been reported. One of them is to immobilize metal complex as the light absorber on the surface of semiconductor substrate. However, in this case, the instability of immobilized metal complexes could be critical issue in the practical application as mentioned above.

1-1-2 Photosensitizer

Photosensitizer (PS) in solar water splitting reaction plays the crucial role in the light absorption to generate excited electron and hole that should be transferred to reduction and oxidation catalysts, respectively. In the process of photo-redox sensitization, there are two different pathways, i.e., "oxidative quenching process" and "reductive quenching process".[14]

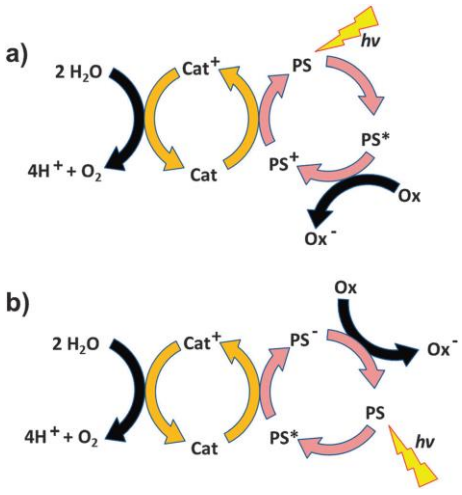

Figure 1-2. a) Oxidative quenching mechanism, and b) reductive quenching mechanism of photo-redox sensitizing process.[14]

As shown in Figure 1-2 a, the oxidative quenching is that the photoexcited PS firstly gives the excited electron to the *reduction* catalyst (it means an oxidation reaction of PS) and the generated one-electron oxidized PS (PS^{+}) returns to the initial normal PS by receiving one electron from the electron donor (*oxidation* catalyst or sacrificial electron donor). In this process, the lifetime of the excited state of PS must be long enough to transfer the electron to catalyst, and the one-electron oxidized species should be stable enough to prevent PS from the decomposition. Conversely, as shown in Figure 1-2 b, reductive quenching is that photoexcited PS firstly receives one electron from electron donor (i.e. reduction reaction of PS) to form one-electron reduced PS ($PS^{\bullet -}$), and then followed by electron transfer from $PS^{\bullet -}$ to reduction catalyst. Consequently, long excited state lifetime and stability in the one-electron reduced species are required in this process. In the studies of half reaction, sacrificial regents (electron donor or acceptor) are generally used to evaluate the photocatalytic activity and durability. In the case of reductive quenching mechanism, it must have long lifetime that not excited state PS but one electron reduction condition PS. In both process, electron transfer efficiency and energy potential level are important. In addition, backward electron transfer need to be inhibited for highly active catalytic reaction because it would occur in every steps. To promote the photocatalytic reaction, the photosensitizer have to become excited state, following reduced state or oxidized state. Thus photosensitizers should have highly durability during the photo excitation and redox reaction.

1-2 Quantum Dot

Quantum Dot (QD) is a very small semiconductor particle, which have only several nanometers. It was firstly reported at 1985 by A. I. Ekimov and A. A. Onushchenko[15]. One of the characteristic features of QD is the wide tunability of both absorption and emission wavelengths by the size of particle (i.e. quantum confined effect) as shown in Figure 1-3. From the view point of development of photosensitizer, controllable absorption, emission wavelength and redox potentials of QD are very attractive to develop a highly efficient solar water splitting system.

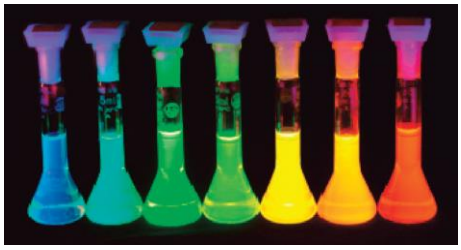

Figure 1-3. Emission of CdSe/ZnS core-shell type Quantum Dot.[16]

In bulk semiconductor, there is a few eV band gap (E_g) between the completely filled VB and the empty CB (Figure 1-4 Bulk Semiconductor). When the semiconductor is irradiated by photon with higher energy than the bandgap, an electron at VB can be excited to CB, enabling to drive some reduction reactions. The remaining hole at VB can also drive some oxidation reactions. Therefore, the band gap energy between VB and CB is one of the crucial parameters for the photosensitizing materials.

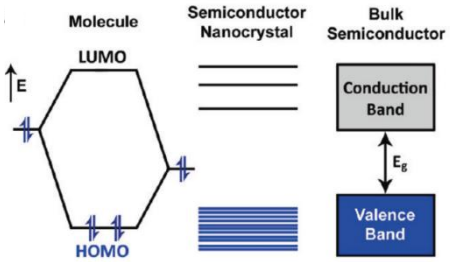

Figure 1-4. Electronic orbital of molecule, band structure of semiconductor nanocrystal and bulk semiconductor. [17]

In contrast, QDs with only several nanometers in size are recently well known to exhibit drastically different photophysical properties from that of the bulk materials. This is basically because

of the quantum confinement effect; the electrons in QDs are fully confined in all three dimensions, leading to form discrete electronic states like those for atoms and molecules instead of band structures for bulk materials (Figure 1-4).[17] The wave function of electron in such the tiny material is given by the following eq. 1-1 and the energy of electron is also given by the eq. 1-2.

$$\psi(x) = \sqrt{\frac{2}{L}} \sin \frac{n\pi x}{L} \qquad \text{eq. 1-1}$$

$$E(n) = \frac{\hbar^2}{2m_e} \left(\frac{n\pi}{L}\right)^2 \qquad \text{eq. 1-2}$$

Here, L denotes the size of nanoparticle, n denotes quantum number, m_e denotes weight of electron. From these formula, the energy of nanoparticle depends on the size of nanoparticle (L) and become discretely.

Various types of QDs have been developed so far, for example Si, Ge (IV semiconductor compound based QD), ZnE, CdE (E = S, Se, Te; II-VI semiconductor compound based QD), InX, GaX (X = P, As; III-V semiconductor compound based QD), PbE (E = S, Se, Te; IV-VI based QD). All of these QDs exhibit size-dependent photo-absorption properties, but the energies at the conduction band minimum and the valence band maximum are determined by the structural components of QDs. Thus, the redox potentials can be also controlled by proper selection of the composed elements of QD. In addition, recent progress in the synthesis semiconductor nanoparticle enable us to prepare not only the nanoparticle with spherical shape, but also with rod-like structure (so called as Quantum Rod). Such semiconductor nanoparticles with anisotropic structures are recently found to be promising method to improve the photosensitizing efficiency.[18] Further, core-shell structure and dot-in-rod structure are also attracting method to enhance not only photosensitizing efficiency, but also the stability of the nano-sized crystals. These features make QDs more fascinating materials for solar water splitting system.

1-3 Quantum Dot/Rod in Photocatalytic Water Splitting Reaction

Researches of photocatalytic H_2 evolution reaction using QD as photosensitizer have been extensively done from 2010's. QD is one of the most attractive photosensitizers because of photophysical properties described above. Considering the photocatalytic H_2 evolution reaction should be driven by sunlight, photosensitizer must absorb visible light. From this viewpoint, cadmium-chalcogenide QDs are widely used as the photosensitizer because of their suitable band gap energy to absorb Visible light. Various types of H_2 evolution catalysts, metal complex, hydrogenase, Pt colloid, have been used with CdE QDs to build homogeneous and heterogeneous H_2 evolving photocatalysts.

QDs were widely used for solar cells. In QD-based solar cells, QDs are used as the light harvesting material and are immobilized on the surface of electrode.[19] Excited electron and hole pair generated in QDs by light absorption are separated to two different electrodes (anode and cathode), resulting in the photocurrent. To utilize the mechanism of solar cell to water splitting reaction, QDs as photosensitizer and both reduction and oxidation catalysts are required to be immobilized on anode and cathode. Photocatalytic water splitting reaction was achieved by modification of the solar cell system.[20] In such systems, QDs were synthesized by chemical bath deposition or electrochemical deposition, no surface passivating ligand is required.

To apply the QDs as the photosentitizer (and/or photocatalyst) for homogeneous photocatalytic water splitting, most of QDs are synthesized in solution phase. One of the examples is the "hot injection method". In this method, surface passivating ligands which covers the surface of QDs to suppress the aggregation are necessary. QDs must be covered by surface passivating ligands with highly hydrophilic functional group like carboxyl and hydroxyl groups to retain the dispersibility to aqueous media. Thus, simple thiol ligands, for example 3-mercaptopropanoic acid (MPA) or 2-mercaptoethanol (MCE), have been used as the surface passivating ligands of photosensitizing QDs. Especially, MPA is one of the most widely used ligands to afford hydrophilic QDs. For example, the systems using hydrogenase as H_2 evolution catalyst were reported about CdTe-MPA QDs[21], CdSe-MPA QDs[21a,21b], CdS-MPA Quantum Rods[22] by Wu group and King group. The system using metal complex as H_2 evolution

catalyst were reported about CdTe-MPA QDs[23], CdSe-MPA QDs[24]. In addition, one of photocatalytic H_2 evolution systems is Pt-modified CdSe-MPA Quantum Rod reported by M. Zamkov group. The CdS nanorod encapsulates CdSe QD to form the Type-II dot-in-rod structure which certainly improves the charge separation efficiency. In the dot-in-rod structure, photoexcited electron can delocalize in the CB of CdS nanorod, leading to the efficient H_2 evolution reaction by Pt colloid. The hole tends to localize in the inner CdSe nanodot and consumed by the electron donation from sacrificial electron donor. From these reports, QDs could be used for all type of H_2 evolution system. In these system, the surface passivating ligand did not affect the mechanism of H_2 evolution reaction and protected the surface of QDs or acted as sacrificial electron donor.

On the other hand, in the system using a metal salt as a precursor of H_2 evolution catalysts, the surface passivating ligands affect the mechanism of hydrogen evolution reaction (HER). For example, Eisenberg *et al*. also reported that a molecular Ni-DHLA species acted as active photocatalytic H_2-evolving catalyst in the presence of CdSe QDs covered with dihydrolipoic acid (DHLA) and a $NiCl_2$ precatalyst and sacrificial electron-donating ascorbic acid, was a molecular Ni-DHLA species (Figure 1-5 (a)).[25] In other instances, Osterloh *et al*. reported the photocatalytic H_2 evolution system contained MCE-covered CdSe QDs as the photosensitizer and Na_2SO_3 as the sacrificial electron donor.[26] They discovered that *in-situ* generated metallic Cd acts as the catalyst for H_2 evolution (Figure 1-5 (b)). However, Wu *et al*. reported a similar photocatalytic HERs.[27] This team used MPA as the surface passivating ligand of the CdSe QDs, $NiCl_2$ as the precursor of the catalyst, and isopropanol as the sacrificial electron donor. In this case, the *in-situ*-generated Ni-CdS layer on the CdSe QD plays an important role in photocatalytic H_2 production (Figure 1-5 (c)).

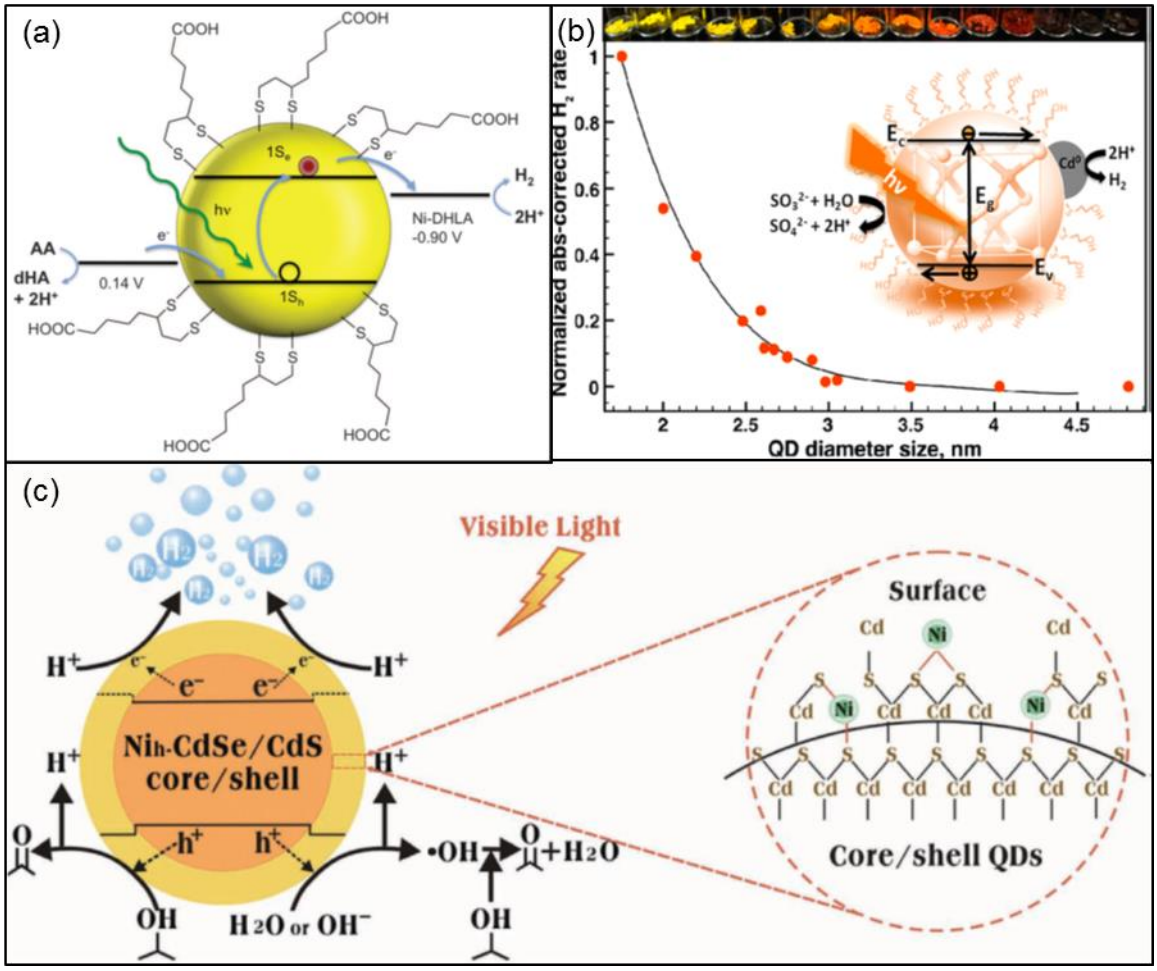

Figure 1-5. The H_2 evolution mechanism of (a) CdSe-DHLA and Ni system, (b) CdSe-MCE system, (c) CdSe-MPA and Ni system.[26, 27, 28]

These recent examples indicate that CdSe QDs have promising photosensitizing ability for solar H_2 production. However, further studies are required, especially on the design of the surface passivating ligands, to improve the photocatalytic activity. Notably, the aforementioned studies employed similar thiolate-based ligands, but the active catalysts were different. The electronic state of a CdSe QD strongly depends on the surface passivating ligand[28]. Thus, the surface passivating ligand on the CdSe QD in a photocatalytic HER plays several key roles in the stabilization and solubilization of the QD as well as in the photoinduced electron transfer pathway and/or formation of the active catalyst.

1-4 Purpose of this study

Extensive studies have revealed the properties of QDs and the role of their surface passivating ligands. In contrast, the relationship between CdSe QDs and the surface passivating ligand in the photocatalytic water reduction is still unclear. Therefore, it should be important that to clarify the role of surface passivating ligand in the water reduction reaction system.

In this study, I synthesized CdSe QDs covered by four different thiols as the surface passivating ligands, and firstly investigated their photophysical properties of CdSe QDs. Secondly, I investigated photocatalytic H_2 evolution reactions using these thiol-covered CdSe QDs as photosensitizer. In the photocatalytic H_2 evolution reactions, polyvinylpyrrolidone-protected Pt colloid (Pt-PVP) or $NiCl_2$ were used as the H_2 evolving (pre)catalyst. I investigated the role of surface passivating ligand in H_2 evolution reaction.

1-5 Outline of the thesis

This thesis consists of three-chapters including this chapter as Chapter 1.

In Chapter 2, CdSe-4-MBA, CdSe-MPA and CdSe-MMBA were synthesized by using hot injection method and exchanging surface passivating ligand. Obtained CdSe QDs were characterized by using powder X-ray diffraction, transmission electron microscopy, absorption and emission spectra, X-ray photoelectron spectroscopy. After characterization, these CdSe QDs were used the photoinduced H_2 evolution reaction as photosensitizer. This reaction solution included Pt-PVP as H_2 evolution catalyst and L-ascorbic acid as sacrificial electron donor. To discuss the H_2 evolution mechanism, dynamic light scattering about mixed solution of CdSe QDs and Pt-PVP and emission spectra about CdSe-MPA with and without Pt-PVP were measured.

In Chapter 3, CdSe-4-MBA, CdSe-MPA and CdSe-3-MBA were synthesized by using hot injection method and exchanging surface passivating ligand. Obtained CdSe QDs were characterized by using powder X-ray diffraction, absorption and emission spectra, X-ray photoelectron spectroscopy. After characterization, these CdSe QDs were used the photoinduced H_2 evolution reaction as photosensitizer. This reaction solution included $NiCl_2$ as precursor of H_2 evolution catalyst and L-ascorbic acid as sacrificial electron donor. To discuss the H_2 evolution mechanism,

In Chapter 4, summary and prospects of the study are described.

References

[1] a) N. S. Lewis, D. G. Nocera, *Proc. Natl. Acad. Sci.* **2006**, *103*, 15729-15735. b) S. Berardi, S. Drouet, L. Francàs, C. Gimbert-Suriñach, M. Guttentag, C. Richmond, T. Stoll, A. Lobet, *Chem. Soc. Rev.*, **2014**, *43*, 7501-7519.

[2] A. Fujishima, K. Honda, *Nature*, **1972**, *238*, 37-38.

[3] P. Du, R. Eisenberg, *Energy Environ. Sci.*, **2012**, *5*, 6012-6021.

[4] A. Kudo, Y. Miseki, *Chem. Soc. Rev.*, **2009**, *38*, 253-278.

[5] a) H. Ozawa, K. Sakai, *Chem. Commun.*, **2011**, *47*, 2227-2242. b) K. Sakai, H. Ozawa, *Coord. Chem. Rev.* **2007**, *251*, 2753-2766.

[6] Y. Halpin, M. T. Pryce, S. Rau, D. Dini, J. G. Vos, *Dalton Trans.*, **2013**, *42*, 16243-16254.

[7] S. Losse, J. G. Vos, S. Rau, *Coord. Chem. Rev.*, **2010**, *254*, 2492-2504. b)

[8] a) S. Fukuzumi, T. Kobayashi, T. Suenobu, *Angew. Chem. Int. Ed.*, **2011**, *50*, 728-731.

[9] W. T. Eckenhoff and R. Eisenberg, *Dalton Trans.*, **2012**, *41*, 13004-13021.

[10] a) H. N. Kagalwala, E. Gottlieb, G. Li, Tao Li, R. Jin, S. Bernhard, *Inorg. Chem.*, **2013**, *52*, 9094-9101. b) Z. Han, L. Shen, W. W. Brennessel, P. L. Holland, R. Eisenberg, *J. Am. Chem. Soc.*, **2013**, *135*, 14659-14669.

[11] L. Duan, F. Bozoglian, S. Mandal, B. Stewart, T. Privalov, A. Llobet, L. Sun, *Nat. Chem.*, **2012**, *4*, 418-423.

[12] E. A. Karlsson, B.-L. Lee, T. Åkermark, E. V. Johnston, M. D. Kärkäs, J. Sun, Ö. Hansson, J.-E. Bäckvall, B. Åkermark, *Angew. Chem., Int. Ed.*, **2011**, *50*, 11715-11718.

[13] M. L. Rigsby, S. Mandal, W. Nam, L. C. Spencer, A. Llobet, S. S. Stahl, *Chem. Sci.*, **2012**, *3*, 3058-3062.

[14] P. D. Frischmann, K. Mahata, F. Würthner, *Chem. Soc. Rev.*, **2013**, *42*, 1847-1870.

[15] A. I. Ekimov, Al. L. Efros, A. A. Onushchenko, *Solid State Commun.*, **1985**, *56*, 921-924.

[16] D. V. Talapin, J.-S. Lee, M. V. Kovalenko, E. V. Shevchenko, *Chem. Rev.*, **2010**, *110*, 389-458.

[17] A. M. Smith, S. Nie, *Accounts of Chemical Research*, **2010**, *43*, 190-200.

[18] H. Zhu, N. Song, H. Lv, C. L. Hill, T. Lian, *J. Am. Chem. Soc.*, **2012**, *134*, 11701-11708.

[19] a) L. C. Kao, S. Y. H. Liou, C. L. Dong, P. H. Yeh, C. L. Chen, *ACS Sustainable Chem. Eng.*, **2016**, *4*, 210-218. b) A. Kondo, G. Yin, N. Srinivasan, D. Atarashi, E. Sakai, M. Miyauchi, *Nanoscale*, **2015**, *7*, 12510-12515. c) J. Li, S. K. Cushing, P. Zheng, T. Senty, F. Meng, A. D. Bristow, A. Maniavannan, N. Wu, *J. Am. Chem. Soc.*, **2014**, *136*, 8438-8449. e) S. Kelekar, C. Ballal, A. Deshpande, S. Warule, S. Ogale, *J. Mater. Chem. A*, **2013**, *1*, 12426-12431.

g) L. Zhu, W.-J. An, J. W. Springer, L. B. Modesto-Lopez, S. Gullapalli, D. Holten, M. S. Wong, P. Biswas, *Inter. J. Hydrog. Energy*, **2012**, *37*, 6422-6430. h) H. M. Chen, C. K. Chen, C. C. Lin, R.-S. Liu, H. Yang, W.-S. Chang, K.-H. Chen, T.-S. Chan, J.-F. Lee, D. P. Tsai, *J. Phys. Chem. C*, **2011**, *115*, 21971-21980. i) H. M. Chen, C. K. Chen, Y.-C. Chang, C.-W. Tsai, R.-S. Liu, S.-F. Hu, W.-S. Chang, K.-H. Chen, *Angew. Chem. Int. Ed.*, **2010**, *49*, 5966-5969.

[20] a) R. Adhikari, L. Jin, F. Navarro-Pardo, D. Benetti, B. AlOtaibi, S. Vanka, H. Zhao, Z. Mi, A. Vomiero, F. Rosei, *Nano Energy*, **2016**, *27*, 265-274. b) V. González-Pedro, I. Zarazua, E. M. Barea, F. Fabregat-Santiago, E. de la Rosa, I. Mora-Seró, S. Giménez, *J. Phys. Chem. C*, **2014**, *118*, 891-895. c) X. Wu, J. Zhao, S. Guo, L. Wang, W. Shi, H. Huang, Y. Liu, Z. Kang, *Nanoscale*, **2016**, *8*, 17314-17321. d) H. B. Yang, J. Miao, S.-F. Hung, F. Huo, H. M. Chen, B. Liu, *ACS Nano*, **2014**, *8*, 10403-10413. e) C. Liu, J. Tang, H. M. Chen, B. Liu, P. Yang, *Nano Lett.*, **2013**, *13*, 2989-2992.

[21] a) K. A. Brown, S. Dayal, X. Ai, G. Rumbles, P. W. King, *J. Am. Chem. Soc.*, **2010**, *132*, 9672-9680. b) F. Wang, W.-G. Wang, X.-J. Wang, H.-Y. Wang, C.-H. Tung, L.-Z. Wu, *Angew. Chem. Int. Ed.*, **2011**, *50*, 3193-3197. c) L.-Z. Wu, B. Chen, Z.-J. Li, C.-H. Tung, *Acc. Chem. Res.*, **2014**, *47*, 2177-2185. d) M. Wen, X.-B. Li, J.-X. Jian, X.-Z. Wang, H.-L. Wu, B. Chen, C.-H. Tung, L.Z. Wu, *Scientific Reports*, **6**, 29851. e) B. L. Greene, C. A. Joseph, M. J. Maroney, R. B. Dyer, *J. Am. Chem. Soc.*, **2012**, *134*, 11108-11111.

[22] K. A. Brown, M. B. Wilker, M. Boehm, G. Dukovic, P. W. King, *J. Am. Chem. Soc.*, **2012**, *134*, 5627−5636.

[23] C. Gimbert-Suriñach, J. Albero, T. Stoll, J. Fortage, M.-N. Collomb, A. Deronzier, E. Palomares, A. Llobet, *J. Am. Chem. Soc.* **2014**, *136*, 7655-7661.

[24] J. Huang, K. L. Mulfort, P. Du, L. X. Chen, *J. Am. Chem. Soc.*, **2012**, *134*, 16472-16475.

[25] Z. Han, F. Qiu, R. Eisenberg, P. L. Holland, T. D. Krauss, *Science*, **2012**, *338*, 1321-1324.

[26] J. Zhao, M. A. Holmes, F. E. Osterloh, *ACS Nano*, **2013**, *7*, 4316-4325.

[27] Z.-J. Li, J.-J. Wang, X.-B. Li, X.-B. Fan, Q.-Y. Meng, K. Feng, B. Chen, C.-H. Tung, L.-Z. Wu, *Adv. Mater.*, **2013**, *25*, 6613–6618.

[28] a) P. R. Brown, D. Kim, R. R. Lunt, N. Zhao, M. G. Bawendi, J. C. Grossman, V. Bulović, ASC Nano, 2014, 8, 5863-5872. b) J. Chang, H. Xia, S. Wu, S. Zhang, *J. Mater. Chem. C*, **2014**, *2*, 2939-2943.

Chapter 2

Photo-induced Hydrogen Evolution Reaction Catalyzed by Pt Colloids

2-1 Introduction

To elucidate the role of the surface ligand, I have focused on the photocatalytic activity for HER of photosensitizing CdSe QDs capped by three different thiol ligands (Scheme 1). The ligands used in this study are the widely used 3-mercaptoprpanoic acid (MPA) ligand, 4-mercaptobenzoic acid (MBA; comprises a surface-passivating thiol group and the water-solubilizing carboxyl group at the para-position of thiophenol), and 4-mercaptomethylbenzoic acid (MMBA; comprises a surface-passivating thiol group, a methyl group between the thiol and phenyl groups and the water-solubilizing carboxyl group at the para-position of toluenethiol). In this work, a polyvinylpyrrolidone-protected Pt colloid (Pt-PVP) was used as the H_2 evolution catalyst to compare the photosensitizing efficiency of the three CdSe QDs and clarify the role of the surface passivating ligand in the photoinduced electron transfer pathway.

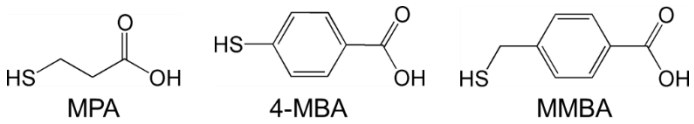

Scheme 2-1. Chemical structures of the surface passivating ligands used in this study: 3-mercaptopropionic acid (MPA), 4-mercaptobenzoic acid (4-MBA), and 4-mercaptomethylbenzoic acid (MMBA).

2-2 Experimental Section

2-2-1 Material and Methods

Materials.

All commercially available starting materials $[Cd(AcO)_2]nH_2O$, Se, tetradecylphosphonic acid (TDPA), hexadecylamine (HDA), tri-*n*-octylphosphine oxide (TOPO), tri-*n*-octylphosphine (TOP), MPA (Sigma-Aldrich), 4-mercaptobenzoic acid (4-MBA), and 10% tetramethylammonium hydroxide aqueous solution, *p*-Toluic acid, *N*-bromosuccinimide, benzoyl peroxide, thiourea, K_2PtCl_4 and polyvinylpyrrolidone (averaged molecular weight is 40000) were used as received, and solvents were used without any purification.

Measurements.

UV-Vis absorption and emission spectra were recorded on a Shimadzu MultiSpec-1500 spectrophotometer and a JASCO FP-6600 spectrofluorometer, respectively, using a 1 cm path length quartz cell. Powder X-ray diffraction patterns were recorded on a Bruker D8 Advance diffractometer equipped with a graphite monochromator using Cu-*K*α radiation and a one dimensional LinxEye detector. X-ray Photoelectron Spectroscopy were performed on a JPC-9010MC using Mg Kα excitation. Transmittance electron microscopy was recorded on a JEOL 2010 FASTEM (200kV). Dynamic Light Scattering (DLS) and the zeta potentials were measured on an OTSUKA ELSZ-100SCl analyzer; glass cell and standard cell units were used for particle size distribution and zeta potential measurements. The pH of the solutions was controlled by adding sodium hydroxide aqueous solution and dilute hydrochloric acid.

2-2-2 Synthesis of 4-mercaptomethylbenzoic acid (MMBA)[1]

The target compound, MMBA was synthesized according to the literature method with minor modification as follows.[1] *p*-Toluic acid (10.88 g, 80 mmol), *N*-bromosuccinimide (17.10 g, 96 mmol),

and benzoyl peroxide (200 mg, 0.8 mmol) were added to 100 mL of $CHCl_3$. The reaction mixture was refluxed for 14 h at 62 °C. After cooling to room temperature, the precipitate was collected by filtration, washed with hot water (3 × 100 mL) and then dried in vacuum to afford the desired compound, 4-bromomethylbenzoic acid (12.47 g, 57.99 mmol, yield: 72 %).

Obtained 4-bromomethylbenzoic acid (7.50 g, 34.88 mmol), and thiourea (2.65 g, 34.9 mmol) were added to 55 mL of H_2O. The mixture was heated to reflux for 1 h, and then allowed to cool to room temperature. A solution of 10% aqueous NaOH (40 mL) was added and then refluxed again for 1 h. The reaction mixture was cooled to 0 °C and 2 M HCl was added to adjust the pH of the reaction solution to be slightly acidic (about pH 5). A cream white precipitate formed that was isolated by vacuum filtration (4.36 g, 25.92 mmol, yield: 74 %). ^{1}H NMR ($CDCl_3$, 298 K): δ 8.05 (d, 2H, J = 8.24 Hz), 7.43 (d, 2H, J = 8.24 Hz), 3.80 (d, 2H, J = 7.75 Hz), 1.80 (t, 1H, J = 7.81 Hz).

2-2-3 Synthesis of CdSe-TOPO[2]

The target TOPO-passivated CdSe QD was synthesized according to literature method with minor modification as follows.[2] The mixture of TDPA (0.0755 g), TOPO (4.04 g), and HDA (2.50 g) was put into three-necked flask and dried under vacuum for 30 min at 100 °C. Under N_2 atmosphere, Se-TOP solution (prepared by dissolving Se (0.079 g) in TOP (1.0 mL)) added to the reaction solution and the mixture was dried again under vacuum at 100 °C for 10 min.

After N_2 packing in three-necked flask, Cd-TOP solution (prepared by dissolving $Cd(AcO)_2 \cdot nH_2O$ (0.06 g) in TOP (1.5 mL)) were added to the reaction solution at 260 °C and temperature of the reaction solution was cooled to 260 °C suddenly, and solution stirred for 4 min at the same temperature. After the 4-min reaction, the temperature of reaction solution was lowered quickly to room temperature, and then the solution was diluted with 20 mL of hexane. The emerged colorless precipitate was removed by centrifugation to obtain the target CdSe-TOPO dispersed solution. To purify the solution, 30 mL of MeOH was added to the supernatant solution to form red-precipitate. The precipitate was collected by

centrifugation and the almost-colorless supernatant solution was removed. This purification process, i.e. the dispersion in hexane and then precipitation by adding MeOH, was done again. Finally, the precipitate of CdSe-TOPO was dispersed in 2 mL of hexane. The diameter (D) of obtained CdSe QD was estimated by the first exctionic absorption band (λ) observed in UV-vis absorption spectrum using eq. 2-1.[3] The molar excition coefficient (ε) of particles of that was estimated by the diameter from eq. 2-1 using eq. 2-2. [3] The concentration of obtained CdSe QD was estimated by the first excitonic absorption band observed in UV-Vis absorption spectrum using Lambert-Beer's Law (equation 2-3, A: absorbance, C: concentration of QDs particle, L: light path length).

$$D = (1.6122 \times 10^{-9})\lambda^4 - (2.6575 \times 10^{-6})\lambda^3 + (1.6242 \times 10^{-3})\lambda^2 - (0.4277)\lambda + (41.57) \quad \text{eq. 2-1}$$

$$\varepsilon = 5857(D)^{2.65} \quad \text{eq. 2-2}$$

$$A = \varepsilon CL \quad \text{eq. 2-3}$$

2-2-4 Synthesis of thiol covered CdSe QDs[3]

The exchange reaction of the surface passivating TOPO to thiol ligand was performed according to the literature method with minor modification as follows. A mixture of 500 μL hexane solution of CdSe-TOPO (200 nmol of the nanoparticles) and 8 mL of methanol was put in a two-necked flask and degassed by N_2 bubbling for 5 min. The thiol ligand [4-MBA (0.3238 g, 2.2 mmol) / MPA (192 μL, 2.2 mmol) / MMBA (0.3700 g, 2.2 mmol)] was dissolved in 10% aqueous tetramethylammonium hydroxide solution (1.5 mL of) with methanol (8 mL) in another flask, degassed by N_2 bubbling for 5 min, and then added to the two-necked flask containing the CdSe-TOPO dispersed solution. The mixed solution was refluxed at 65 °C overnight under N_2 atmosphere in dark. After cooling to room temperature, ethyl acetate (20 mL) was added to the reaction solution to emerge red precipitates. Obtained precipitates (CdSe-4-MBA / CdSe-MPA / CdSe-MMBA) was collected by centrifugation and the supernatant solution was removed. The precipitate was dispersed in H_2O (2 mL) containing two

drops of 10% tetramethylammonium hydroxide solution. The concentration of obtained CdSe QD was also estimated by the first excitonic absorption band observed in UV-Vis absorption spectrum using equations 2-1, 2-2 and 2-3.

2-2-5 Synthesis of polyvinylpyrrolidone-protected Pt (Pt-PVP) colloid[4]

K_2PtCl_4 (66.41 mg, 160 μmol) and Polyvinylpyrrolidone (177.7 mg,1.6 mmol) were dissolved in EtOH (420 mL) in dark. The solution was refluxed for 3 hour at 80 °C. After cooling to room temperature, the reaction solution was evaporated to dryness. Obtained black film-like solid was dispersed in H_2O (10 mL) to remove KCl, one of the main byproducts. The black solution was centrifuged and the supernatant solution was removed. Obtained black film-like solid was again washed by H_2O (10 mL) and re-collected by centrifugation as the same procedure. Finally, the black precipitates of the target PVP-protected Pt colloids (Pt-PVP) were dispersed in H_2O (200 mL). The averaged diameter of obtained Pt-PVP colloid was estimated to be 3.1 nm by the peak fitting of powder X-ray diffraction pattern using Scherrer equation.[5]

2-2-6 Photocatalytic hydrogen evolution reaction

Samples were prepared in 40 mL vials and protected from light before use. A 2.7 μM Pt-PVP colloid, 4.0 μM CdSe-QDs (CdSe-4-MBA/ CdSe-MMBA / CdSe-MPA), and 0.5 M ascorbic acid in H_2O were added to form a total volume of 4.5 mL. The pH of the solutions was adjusted by the addition of aqueous 2 M HCl or 2 M NaOH solution. The samples were sealed with an airtight cap equipped with two rubber septa and then degassed by N_2 bubbling for 1 h. The samples were irradiated from below the vials with OP6-5310HP2 visible light LEDs (λ = 525 nm, Opt-Device Laboratory Ltd). The light power of each LED was set to 40 mW and measured with a COHERENT FieldMaxII-TO laser power meter. During the photoreaction, the samples were stirred using a stirrer tip. The gas in the top-space of the vials was collected using a HAMILTON Microlab 600 auto-dispenser and injected to an

Agilent 490 MicroGC gas chromatograph to measure the amount of hydrogen evolved.

2-3 Results and Discussion

2-3-1 Powder X-ray diffraction and transmission electron microscopy

Powder X-ray diffraction patterns of four CdSe QDs are shown in Figure 2-1. All CdSe QDs exhibited very broad but similar diffraction patterns to that of bulk CdSe (wurtzite), indicating that the crystal structures of all four CdSe QDs are the same to the bulk, i.e., the zinc blend structure. Their particle diameters were estimated to be almost constant 2.6 ± 0.2 nm by using Scherrer's equation[5] for broad peak including (100), (002) and (101) reflection. In the case of CdSe-TOPO, the estimated particle size was also comparable to the size of CdSe-TOPO evaluated by transmission electron microscopic (TEM) analysis (see Figure 2-2). This result indicates that the surface ligand exchange reactions from TOPO to the four different thiols have little effect on the particle size of CdSe QD.

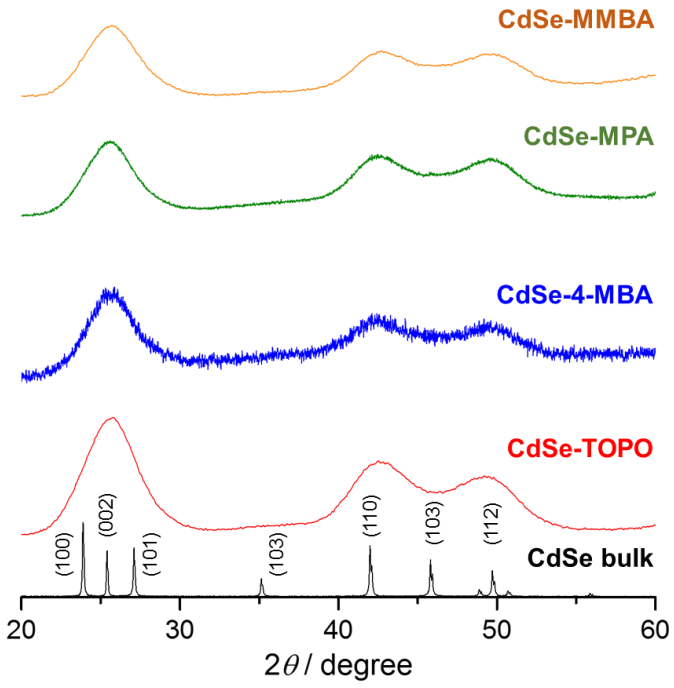

Figure 2-1. Powder X-ray diffraction patterns of bulk CdSe (black), CdSe-TOPO (red), CdSe-MBA (blue), CdSe-MPA (green), and CdSe-MMBA (orange).

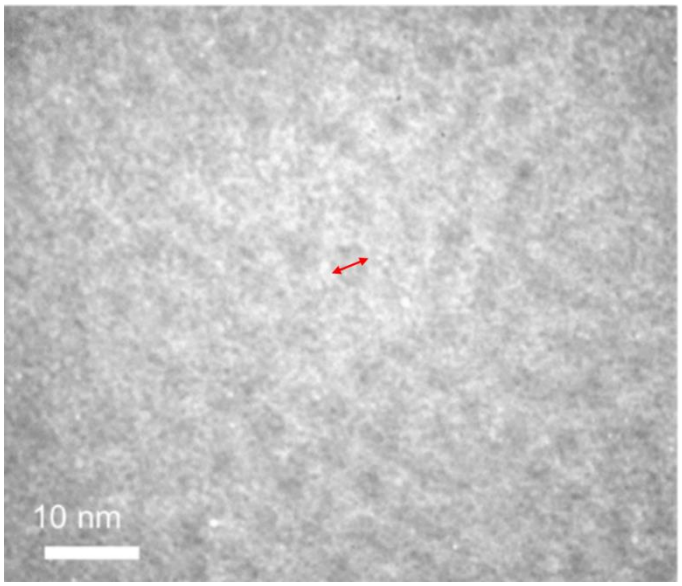

Figure 2-2. TEM image of CdSe-TOPO. The estimated size of one CdSe QD indicated by arrows is about 3.3 nm.

2-3-2 UV-vis Absorption and Emission Property

Figure 2-3 illustrates UV-Vis absorption and emission spectra of the afforded QDs in the dispersed solution state. The particle size of CdSe QDs can be estimated from the first exciton peak.[3] The CdSe-TOPO, CdSe-4-MBA, CdSe-MPA, and CdSe-MMBA QDs exhibited a first exciton peak at almost the same wavelength (listed in Table 2-1), indicating that the particle sizes of these QDs are almost independent of the surface passivating ligand. The small (compared to that of CdSe-TOPO) red shifts of the first exciton peak observed for thiolate-passivated CdSe QDs are not attributed to the change in particle size but to the differences in the electronic state of the surface ligands. Several groups reported that the thiol ligands form stronger coordination bonds on the surface of the CdSe QDs than TOPO. This leads to a smaller quantum confinement effect.[6] Thus, the small red shifts observed for CdSe-MPA, CdSe-4-MBA, and CdSe-MMBA are attributed to the same reaction mechanism as that of the thiol passivated CdSe QDs reported in literature.

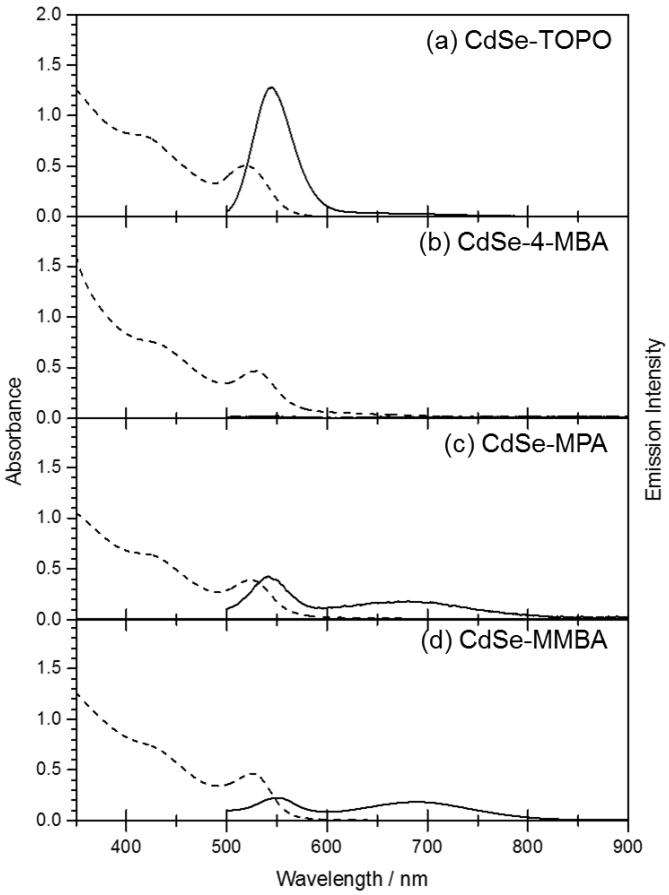

Figure 2-3. UV-Vis absorption (dashed lines) and emission (solid lines) spectra of (a) CdSe-TOPO in *n*-hexane, (b) CdSe-4-MBA, (c) CdSe-MPA, and (d) CdSe-MMBA in basic water; λ_{ex} = 400 nm.

Table 2-1. Absorption and emission peaks for the afforded CdSe QDs.

CdSe QDs	Absorption / nm	Emission / nm
CdSe-TOPO	518.4	543.4
CdSe-4-MBA	528.7	n. d.
CdSe-MPA	523.6	541.2, 680.8
CdSe-MMBA	525.0	546.2, 687.6

CdSe QDs are generally known as strong emitters, but their luminescence quantum yields strongly depend on the surface ligand. Strong band-edge fluorescence was observed at 543 nm for CdSe-TOPO, whereas the three thiolate-passivated CdSe QDs only exhibited weak band-edge emissions (Figure 2-3). The thiol-based surface ligands were reported to trap holes generated in the

valence band (VB) of the CdSe QDs and quench photoluminescence. This is due to the higher HOMO orbital energy of the thiols when compared to the VB energy of the CdSe QDs.[6b, 7] In addition, the efficiency of hole trapping by the thiol ligands depends on the electronic state of the thiol; aromatic thiols tend to trap holes more effectively than aliphatic thiols because the hole in the VB can be delocalized not only on the thiolate group, but also in the aromatic ring.[8] In the case of MMBA, it would be difficult to transfer the hole generated on the VB of CdSe QD to the aromatic ring of MMBA. This is because the methylene spacer interrupts the delocalization of the hole in the aromatic ring. However, a small amount of charge separation still occurs through tunneling effects of the aromatic ring π-electrons.[9] Thus, CdSe-MBA exhibits the weakest band-edge emission, following CdSe-MMBA and CdSe-MPA, respectively.

Notably, the thiolate-passivated QDs displayed another weak and broad emission band at ~680 nm that can be attributed to deep trap emission. Kamat *et al.* reported that Se-vacant sites are formed on the surface of the CdSe QDs when an MPA surface ligand is added to the system.[10] This results in emission from a deeply trapped state. The MPA-passivated CdSe QDs clearly display a lower-energy broad emission assignable to the deep trap emission from the Se-vacant site at 680 nm (Figure 2-3). The CdSe-MMBA QD also exhibits a similar emission spectrum. In contrast, CdSe-4-MBA did not exhibit any emission in this range, suggesting that the electron transfer quenching by the MBA ligands are more effective than that of the other two ligands. These results clearly indicate that changing the surface ligand from TOPO to thiolates does not affect the particle size of the CdSe QDs, but the emission behavior of these QDs strongly depends on the electronic nature of the ligand, even among similar thiol derivatives.

2-3-3 X-ray Photoelectron Spectroscopy

As discussed in the previous section, the emission behaviors of two CdSe-4-MBA and the other two are significantly different. In order to investigate the origin of the large difference between

them, X-ray photoelectron spectroscopic (XPS) measurements were conducted. As shown in Figures 2-4 to 2-8, two peaks assignable to the Cd 3d 5/2 and Cd 3d 3/2 photoelectrons are observed at 404 and 411 eV, respectively, bulk size CdSe and all five CdSe QDs. Interestingly, observed peaks for CdSe-MPA are significantly broader than those for CdSe-4-MBA. Considering that almost the same bandwidth to CdSe-4-MBA was also observed for the starting QDs, CdSe-TOPO (Figure 2-4 and Table 2-2), there are at least two different Cd sites in CdSe-MPA and CdSe-MMBA. According to a report by Mulvaney et al., the Cd-rich CdSe QDs show two different XPS peaks in the Cd 3d region, whereas the Se-rich CdSe QDs exhibit only a single peak.[11] In addition, from emission spectra (Figure 2-3), CdSe-MMBA also had Se defect on the surface of CdSe QD. Therefore, we assume that the broadening of the XPS peaks in the Cd 3d region of CdSe-MPA and CdSe-MMBA are due to the contribution of Cd sites near the surface, which are strongly affected by the coordination of the surface-passivating MPA and MMBA ligands. Thus, observed XPS peaks in the Cd 3d region of CdSe-MPA and CdSe-MMBA were analyzed by using two components, *i.e.*, contributions from Cd sites near the surface and inside the core of QD. Conversely, only one component was used for the analysis of XPS spectra of the CdSe-4-MBA, because the peaks were sharp enough to assume that there is only one Cd site like the starting CdSe-TOPO. The fitting results are summarized in Table 2-2, 2-4. The estimated binding energy and the full width at half maximum (FWHM) for CdSe-4-MBA are very similar to those of bulk size of CdSe or CdSe-TOPO. Although the estimated FWHM values for CdSe-MPA and CdSe-MMBA by one-component analysis are larger than that of bulk size of CdSe or CdSe-TOPO, similar FWHM values were obtained by two-component analysis for the spectra of CdSe-MPA and CdSe-MMBA (Table 2-3, 2-5). These contrasting results clearly indicate that the surface conditions of CdSe-4-MBA and the other two thiolate-passivated CdSe QDs are significantly different, despite these thiol-based surface-passivating ligands being introduced under very similar surface-ligand exchange reaction conditions. Thus, the difference could originate from the electronic nature of these ligands. The electron lone pairs of the thiolate groups of MPA and

MMBA are localized only on the thiolate group, resulting in strong coordination to the Cd at the QD surface. In contrast, the electron lone pairs of the thiolate of 4-MBA are delocalized not only on the thiolate, but also on the adjacent phenyl group, which leads to the formation of weaker Cd-S bonds. The stronger Cd-S (MPA) bond formation may remove the Se^{2-} ion at the surface of the QD to form higher numbers of surface Se-vacant sites. This assumption is supported by the emission spectra; the emission derived from the deeply trapped state is not observed in CdSe-4-MBA, but certainly observed in CdSe-MPA and CdSe-MMBA (see Figure 2-3).

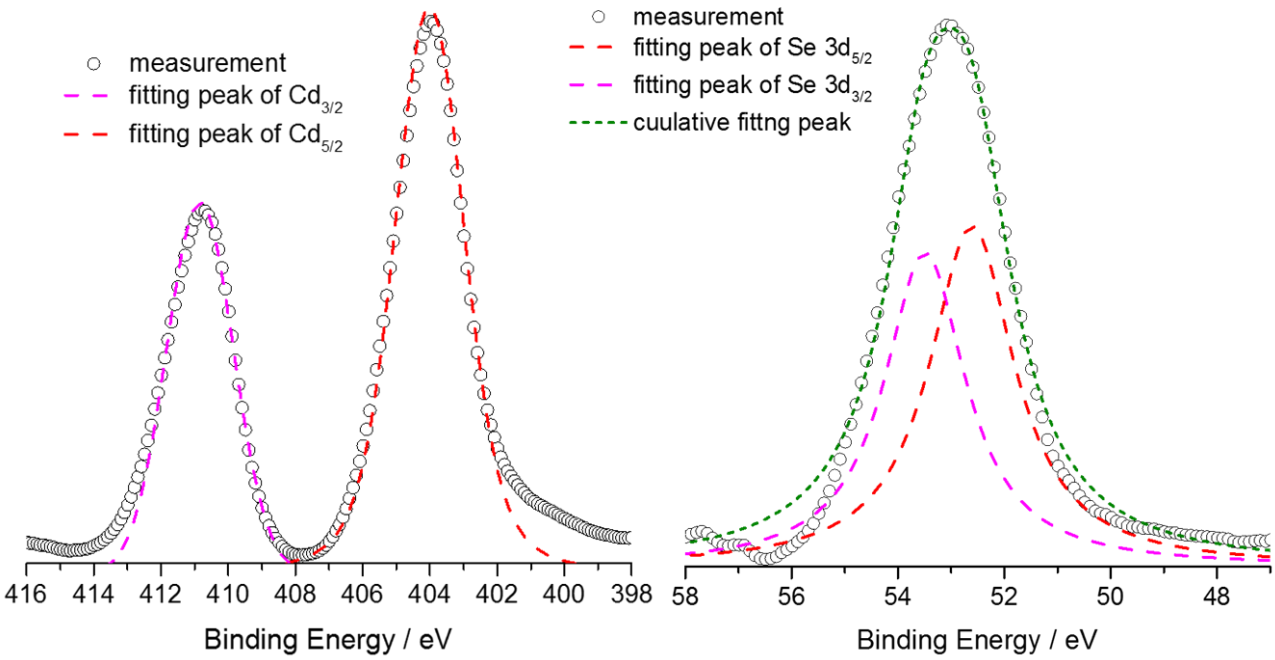

Figure 2-4. XPS spectra of Cd region (left) and Se region (right) of bulk size CdSe

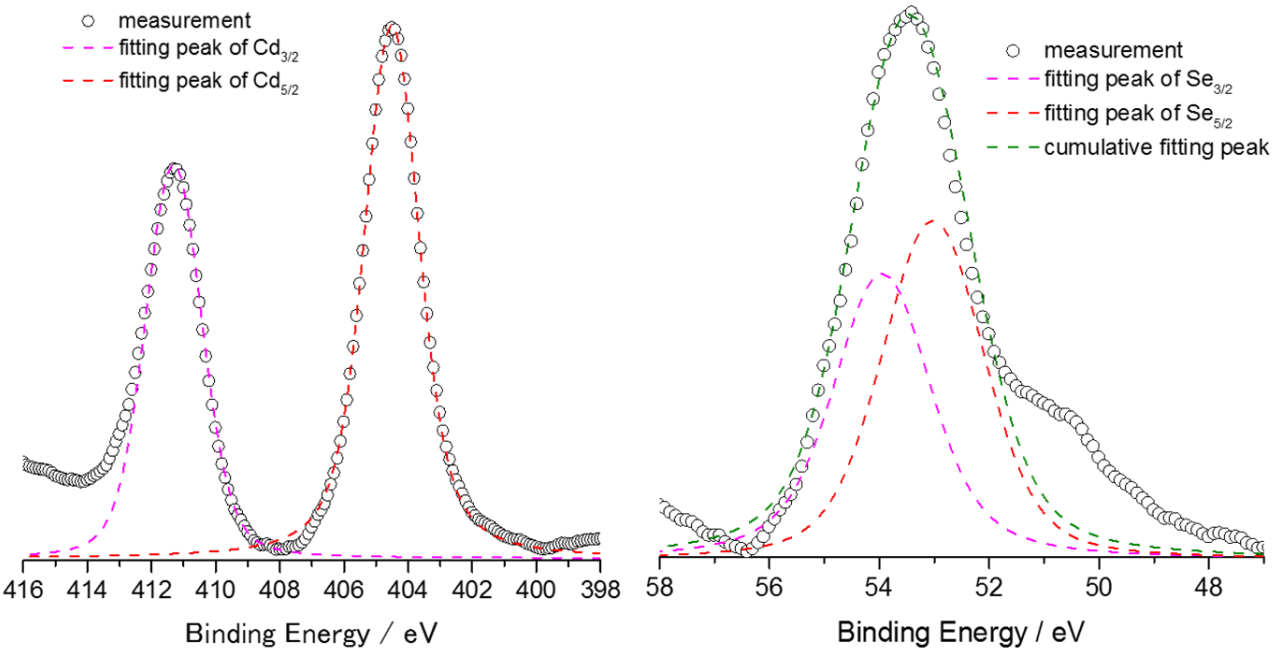

Figure 2-5. XPS spectra of Cd region (left) and Se region (right) of CdSe-TOPO.

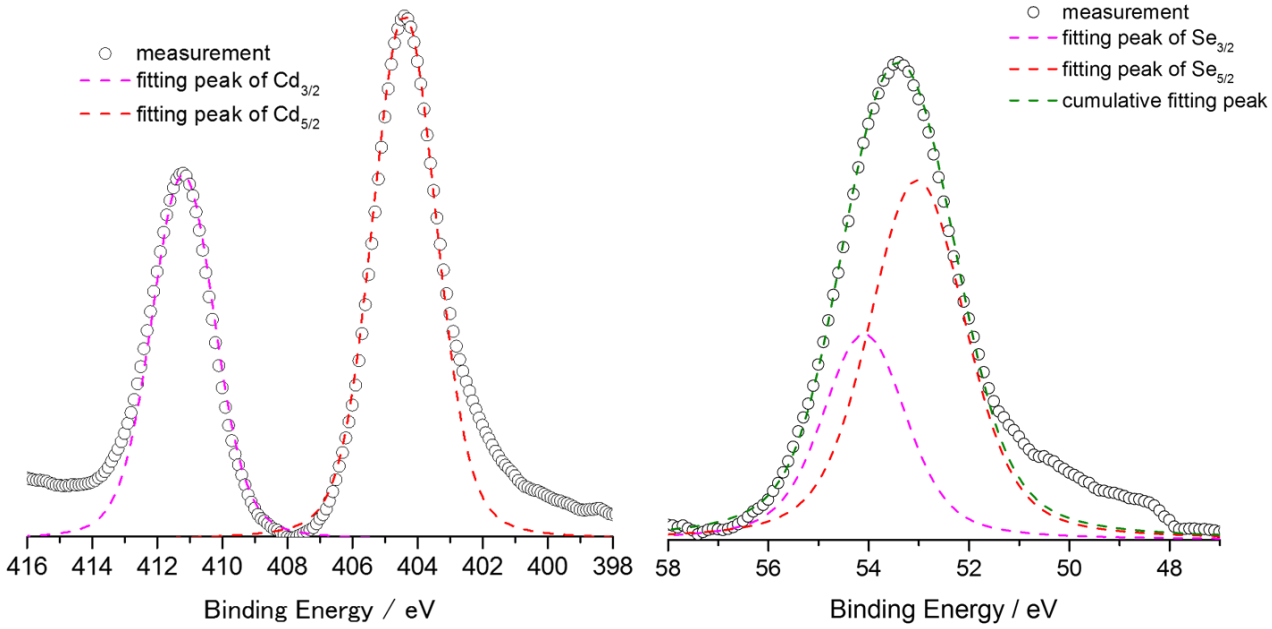

Figure 2-6. XPS spectra of Cd region (left) and Se region (right) of CdSe-4-MBA.

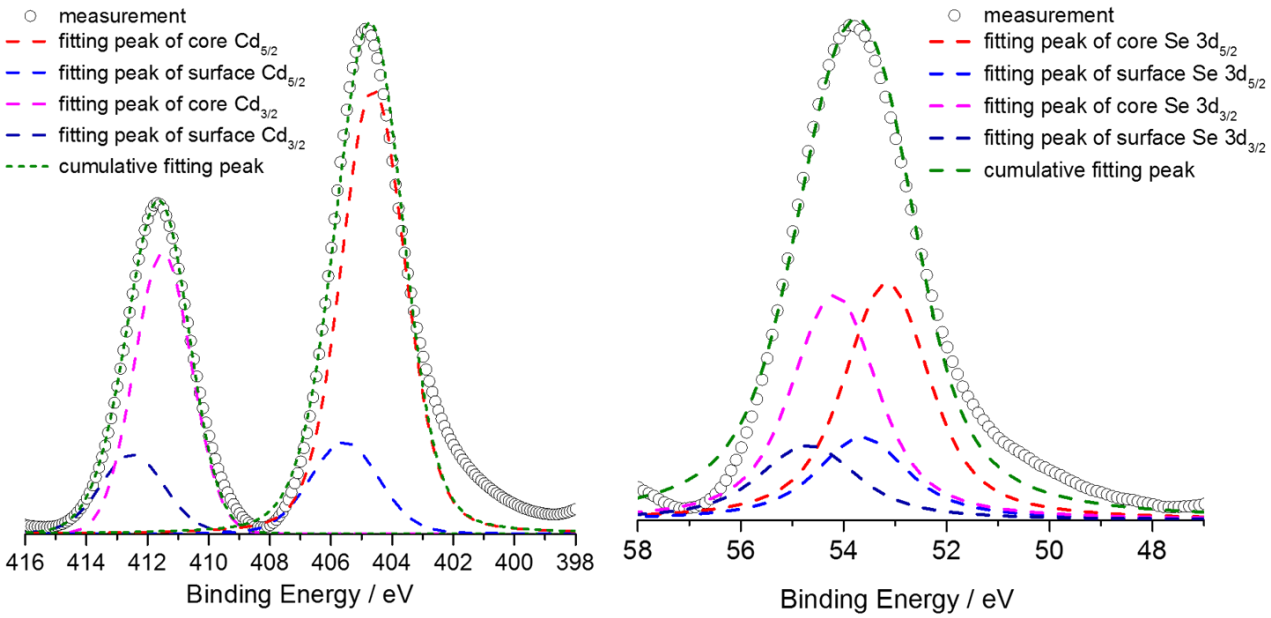

Figure 2-7. XPS spectra of Cd region (left) and Se region (right) of CdSe-MPA.

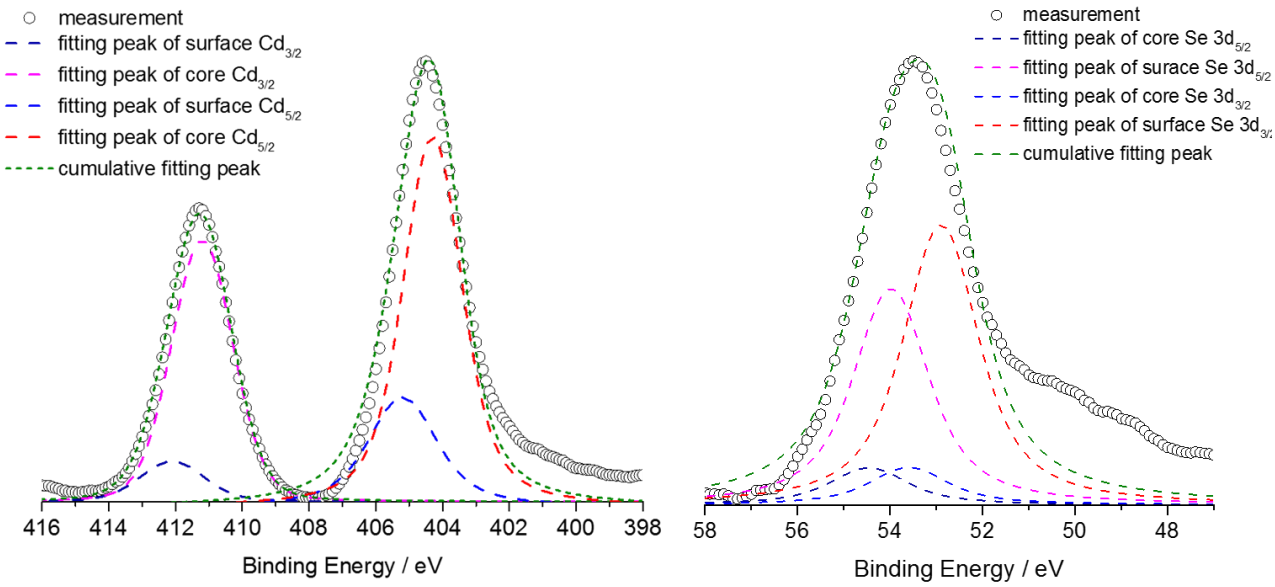

Figure 2-8. XPS spectra of Cd region (left) and Se region (right) of CdSe-MMBA.

Table 2-2. Peak-fitting results based on one-component analysis for XPS spectra in Cd 3d region.

Sample	peak		Binding Energy [eV]	FWHM	Area	%Conc.
CdSe (bulk)	Cd 3d 5/2	Peak 1	404.01	2.460	64702.7	64
	3d 3/2	Peak 1	410.79	2.350	36272.4	36
CdSe-TOPO	Cd 3d 5/2	Peak 1	404.51	2.039	6773.7	59
	3d 3/2	Peak 1	411.31	2.082	4672.0	41
CdSe-4-MBA	Cd 3d 5/2	Peak 1	404.41	2.330	9052.1	59
	3d 3/2	Peak 1	411.21	2.281	6181.2	41
CdSe-MPA	Cd 3d 5/2	Peak 1	404.89	2.654	19997.9	62
	3d 3/2	Peak 1	411.69	2.454	12158.9	38
CdSe-MMBA	Cd 3d 5/2	Peak 1	404.42	2.251	13725.3	69
	3d 3/2	Peak 1	411.29	2.124	6058.9	31

Table 2-3. Peak-fitting results based on two-component analysis for XPS spectra in Cd 3d region.

Sample	peak		Binding Energy [eV]	FWHM	Area	%Conc.
CdSe-MPA Fitting peaks	Cd 3d 5/2	Peak 1	404.62	2.480	17546.7	53
		Peak 2	405.56	2.664	3745.5	11
	Cd 3d 3/2	Peak 1	411.50	2.205	9098.9	27
		Peak 2	412.50	2.465	3018.3	9
CdSe-MMBA Fitting peaks	Cd 3d 5/2	Peak 1	404.30	2.105	9517.5	47
		Peak 2	405.20	2.456	3466.4	17
	3d 3/2	Peak 1	411.20	2.165	6089.6	30
		Peak 2	412.10	2.281	1008.4	6

Table 2-4. Peak-fitting results based on one-component analysis for XPS spectra in Se 3d region.

Sample	peak		Binding Energy [eV]	FWHM	Area	%Conc.
CdSe (bulk)	Se 3d 5/2	Peak 1	52.61	1.942	920.7	50
	3d 3/2	Peak 1	53.49	1.862	925.9	50
CdSe-TOPO	Se 3d 5/2	Peak 1	53.02	2.203	760.1	54
	3d 3/2	Peak 1	53.95	2.105	653.0	46
CdSe-4-MBA	Se 3d 5/2	Peak 1	53.03	2.266	1012.3	66
	3d 3/2	Peak 1	54.09	1.973	515.07	34
CdSe-MPA	Se 3d 5/2	Peak 1	53.43	2.679	1435.7	62
	3d 3/2	Peak 1	54.27	2.364	869.4	38
CdSe-MMBA	Se 3d 5/2	Peak 1	53.03	2.679	1589.2	62
	3d 3/2	Peak 1	53.90	2.510	985.8	38

Table 2-5. Peak-fitting results based on one-component analysis for XPS spectra in Se 3d region.

Sample	peak		Binding Energy [eV]	FWHM	Area	%Conc.
CdSe-MPA Fitting peaks	Se 3d 5/2	Peak 1	53.16	1.965	912.3	72
		Peak 2	53.64	2.102	361.3	28
	Se 3d 3/2	Peak 1	54.18	1.965	867.5	72
		Peak 2	54.69	2.268	343.8	28
CdSe-MMBA Fitting peaks	Se 3d 5/2	Peak 1	53.97	1.942	772.0	38
		Peak 2	54.45	2.021	138.1	7
	3d 3/2	Peak 1	52.89	1.942	988.6	48
		Peak 2	53.59	2.021	139.9	7

2-3-4 Photocatalytic hydrogen evolution reaction

Figure 2-8 illustrates the results of the photoinduced hydrogen evolution reactions driven by the photosensitizing CdSe QD and the Pt-PVP colloidal catalyst in aqueous solution (pH = 6). The reaction solutions comprise 0.5 M ascorbic acid as the sacrificial electron donor (the wavelength of irradiated light = 525 nm). The determined turnover number (TON) and turnover frequency (TOF) for each solution are summarized in Table 2-6. The TON and TOF values decrease in the order: CdSe-MPA > CdSe-4-MBA > CdSe-MMBA, despite the fact that the CdSe QDs have almost comparable particle diameters and first exciton energies. Thus, since the Pt-PVP nanoparticles were the same as those used in the hydrogen evolving catalyst, the large difference in evolved H_2 should originate from differences in the CdSe QDs. After light irradiation for 15 hours, orange precipitates were formed in all three reaction solutions, implying the these three CdSe QDs are not stable enough to maintain the photocatalytic activity for long-time irradiation, probably because of the more labile nature of monothiolate ligand than the other ligands with several thiolate groups.[12]

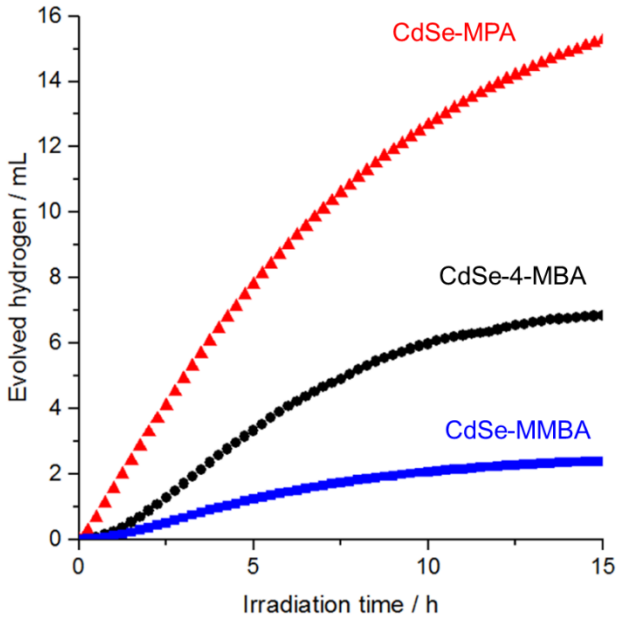

Figure 2-8. Photocatalytic hydrogen evolution reactions (HERs) from aqueous solutions (pH 6) comprising 4 μM CdSe-4-MBA (black circles), CdSe-MPA (red triangles) or CdSe-MMBA (blue squares) as the photosensitizer, ascorbic acid (0.5 M) as the sacrificial electron donor, and Pt-PVP (12 nM) as the hydrogen evolution catalyst; light irradiation at 525 nm.

Table 2-6. Turnover numbers (TON) and maximum turnover frequencies (maxTOF) of photocatalytic hydrogen evolution reactions (HERs) driven by photosensitizing CdSe QDs and a Pt-PVP colloid.

CdSe QD	TON[a]	$_{max}$TOF / h
CdSe-MPA	34000	3900
CdSe-4-MBA	15000	2000
CdSe-MMBA	5400	720

[a.] Turn over numbers per amount of CdSe QD nanoparticles calculated from the amount of hydrogen evolved after irradiation for 15 h.

2-3-5 Dynamic Light Scattering Measurement

To clarify why the photocatalytic activity strongly depends on the surface passivating ligand of the CdSe QD, the dispersibility of the QDs in water was investigated by DLS. Figure 2-9 displays the

distribution of the particle diameters of the three thiolate-passivated CdSe QDs. Notably, the estimated particle diameters of these three QDs are remarkably different, even in the absence of the Pt-PVP colloidal catalyst. The average diameters were estimated by DLS as ~2.0 nm for CdSe-MPA, 51.2 nm for CdSe-4-MBA, and 126 nm for CdSe-MMBA (in water, pH = 6, Table 2-7). This significant difference in particle size is attributed to the difference in the dispersibility of the three CdSe QDs, that is, the formation of aggregates of CdSe QDs. This is confirmed by the UV-vis absorption spectra (Figure 2-3) that clearly indicate that the diameter of one CdSe QD is comparable among all three CdSe QDs. The electrostatic interactions between the particles are crucial for the dispersibility of the particles in water, i.e., highly charged particles are well dispersed in water because of the electrostatic repulsion between them. As a result, CdSe-MPA exhibited better dispersibility in an aqueous solution (pH 6), probably because it depended on the bulkiness of the surface passivating ligand (molecular volume: MPA = 86.07 $Å^3$, 4-MBA = 122.73 $Å^3$, MMBA = 140.05 $Å^3$). This hypothesis is also supported by the pH dependence of the average particle sizes of CdSe-MPA and CdSe-4-MBA; the large aggregates (over 1000 nm) were observed at pH = 5 for CdSe-4-MBA, but the aggregation occurred at lower pH (pH = 4) for CdSe-MPA (Figure 3-3). When these surface passivating ligands covered same-sized QDs, the number of 4-MBA or MMBA moieties was less than that of MPA because both 4-MBA and MMBA are bulkier than MPA. In addition, the methylene group between the thiolate and phenyl groups of MMBA ligand would increase the actual molecular volume due to the free rotation along the C-C bonds at the methylene group. Thus, a reduction in surface negative charge density (a property that requires good dispersibility) was observed, while the dispersibility of both 4-MBA and MMBA became worse.

These observations were supported by the zeta potential values where CdSe-MPA displayed the largest negative charge followed by CdSe-4-MBA and CdSe-MMBA, respectively (pH = 6 aqueous solution, Table 2-7). Moreover, after the Pt-PVP colloid (12 nM) was added to the CdSe QD-dispersed solution, the average sizes of CdSe-MPA and CdSe-4-MBA increased to 1645 nm and 461 nm,

respectively, while a negligible decrease in the size of CdSe-MMBA was observed. Considering that Pt-PVP has a zeta potential of +2.6 mV, the increasing average sizes of CdSe-MPA and CdSe-4-MBA, following the addition of the Pt-PVP colloid, was due to aggregate formation between Pt-PVP and CdSe-MPA/CdSe-4-MBA by electrostatic interactions between the negatively charged CdSe QD and the positively charged Pt-PVP colloid. This is supported by the plots in Figure 2-9 that illustrate that the addition of a PVP polymer without a Pt colloid did not alter the average size (measured by DLS) of the CdSe QD. Moreover, the addition of Pt-PVP caused a positive shift in the zeta potentials of both CdSe-MPA and CdSe-4-MBA (Table 2-7). Conversely, the addition of the Pt-PVP colloid did not affect the average size of CdSe-MMBA. This occurs for two main reasons, namely, the negative charge of CdSe-MMBA is smaller than those of both CdSe-MPA and CdSe-4-MBA, and CdSe-MMBA already undergoes aggregation in the absence of Pt-PVP.

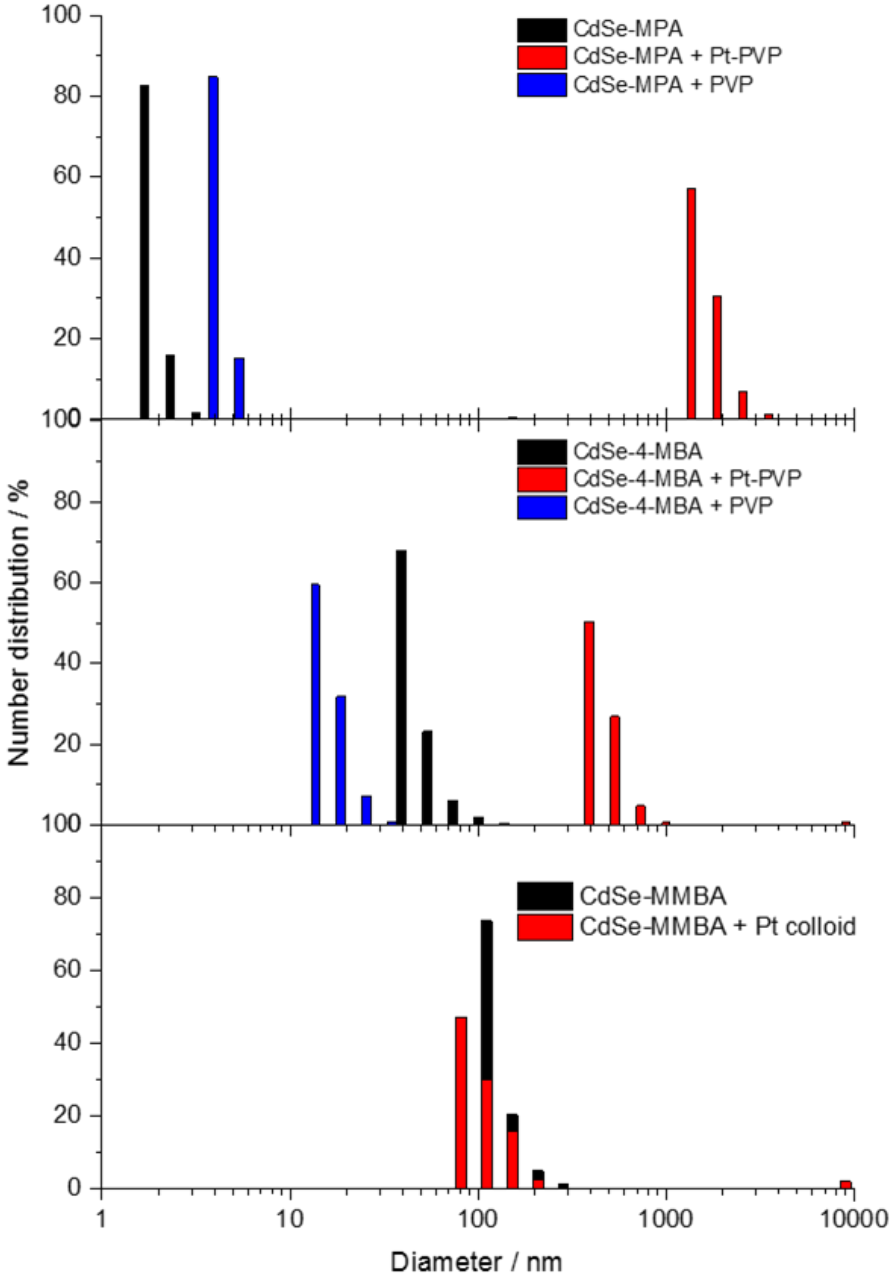

Figure 2-9. Particle diameter distributions estimated by dynamic light scattering (DLS) of CdSe-MPA (top), CdSe-4-MBA (middle), and CdSe-MMBA (bottom), dispersed in water (pH = 6) before (black) and after addition of a Pt-PVP colloidal solution (red) or PVP polymer (blue, 4.95 mM as the monomer unit). The particle concentrations of the CdSe QD and Pt-PVP colloid are 4.0 μM and 12.0 nM, respectively.

Table 2-7. Average particle diameter and zeta potential of CdSe QDs in the dispersed aqueous solution.

	aqueous solution (pH 6)		**+ 12 nM Pt-PVP colloida**	
	Average diameter / nm	ζ potential / mV	Average diameter / nm	ζ potential / mV
CdSe-MPA	2.0	–38.37 mV	1645	–13.94 mV
CdSe-4-MBA	51.2	–29.79 mV	461	–19.39 mV
CdSe-MMBA	126	–20.59 mV	107	–17.39 mV

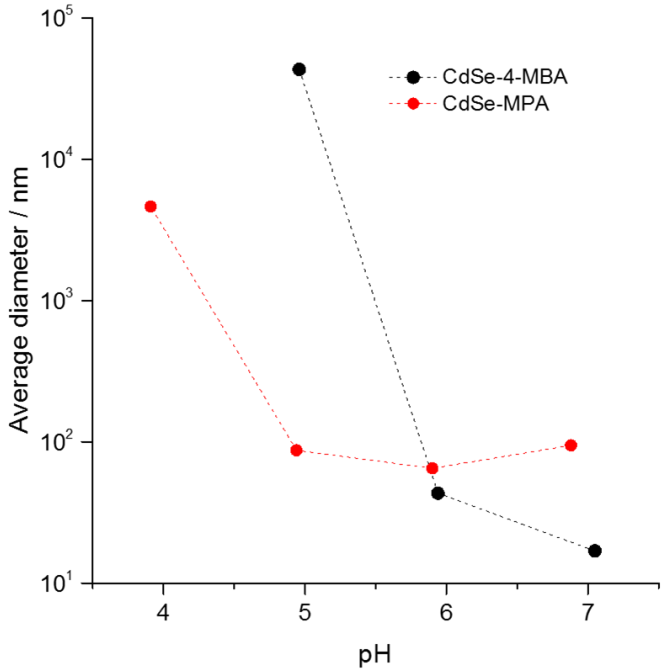

Figure 2-10. pH dependences of the averaged particle diameters of (red) CdSe-MPA and (black) CdSe-4-MBA estimated by DLS measurements in aqueous solution.

2-3-6 Quenching Experiment

A luminescence quenching experiment was conducted to clarify the effect of the aggregation of CdSe-MPA and the Pt-PVP colloid on the photophysical properties of the CdSe QD. Figure 2-11 illustrates the changes in the luminescence spectrum of CdSe-MPA caused by the addition of the Pt-PVP colloid, or ascorbic acid, as the luminescence quencher. As discussed in the section 2-3-2, CdSe-MPA exhibits a sharp band-edge emission at 524 nm and a broad emission originating from the surface

Se-defect at 680 nm. Interestingly, both the emission derived from the Se-defect and the band-edge fluorescence completely disappear after the addition of the Pt-PVP colloid. Notably, the concentration of the colloid was only one-tenth of that used in the photocatalytic HER. The formation of aggregates composed of CdSe-MPA and Pt-PVP colloids was confirmed by DLS measurements even in more diluted concentrations of the Pt-PVP colloid (Figure 2-11). These results clearly indicate that the luminescence of the CdSe QD was effectively quenched in the aggregate comprising the Pt-PVP colloid. This is probably due to electron transfer from the photoexcited CdSe QD to the Pt-PVP colloidal catalyst (oxidative quenching mechanism). The complete quenching of the emission from Se-defect site by Pt-PVP colloid was also observed at the different pH conditions (pH = 5, 6 and 8, Figure 2-13). On the other hand, although similar emission quenching was observed in the presence of ascorbic acid as the sacrificial electron donor, the quenching efficiency was found to be less than that of the Pt-PVP colloid. The intensity of broad Se-defect emission decreased by 30% in the presence of an ascorbic acid quencher (20 mM), and it was almost completely quenched in the presence of a much more concentrated (0.4 M) ascorbic acid solution. Notably, the band-edge emission of CdSe-MPA was still observed in the 0.4 M ascorbic acid solution whereas it was completely quenched in the presence of the 12 nM Pt-PVP colloid. Taking into consideration that the concentrations of the Pt-PVP colloidal catalyst and sacrificial electron-donating ascorbic acid in the photocatalytic HERs were 12 nM and 0.5 M, respectively, there are two possible photoinduced electron transfer mechanisms. In the first mechanism, the photoexcited CdSe-MPA donates the excited electron to the Pt-PVP colloidal catalyst. The oxidized CdSe-MPA is then regenerated by electron transfer from ascorbic acid (sacrificial electron donor). The second mechanism is the inverse process, that is, the photoexcited CdSe-MPA first receives an electron from the ascorbic acid, after which, the one-electron-reduced CdSe donates an electron to the Pt-PVP colloidal catalyst. Since CdSe-MPA forms aggregates with the Pt-PVP colloid, the former mechanism would be dominant for the CdSe-MPA directly attached to Pt-PVP colloid, whereas the latter process would be more dominant for the CdSe-MPA present near the surface

of the aggregate. This occurs because of easier access to the ascorbic acid in the aqueous solution. We also confirmed that the Se-defect emission of CdSe-MMBA was completely quenched in the presence of the Pt-PVP colloid (1.2 nM, one-tenth of the concentration of the photocatalytic HER, Figure 2-14). This suggests that an electron transfer pathway similar to that of CdSe-MPA would contribute toward the photocatalytic HER and the difference of molecular length of the surface passivating ligands MMBA and MPA would not affect significantly on the emission quenching efficiency.

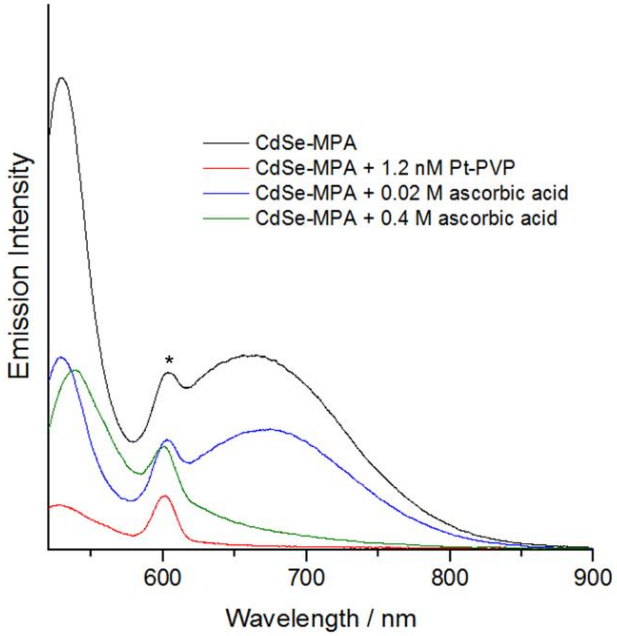

Figure 2-11. Emission spectra of CdSe-MPA (black, 1.4 μM), in the presence of 1.2 nM Pt-PVP colloid (red), and 0.02 M (blue) or 0.4 M ascorbic acid (green). The peaks indicated by the asterisk are attributed to Raman scattering of the water solvent; λ_{ex} = 500 nm.

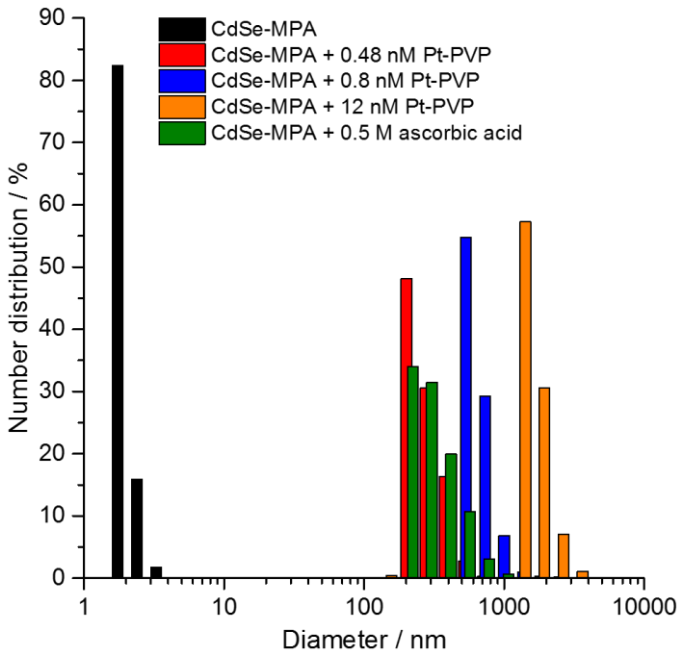

Figure 2-12. Particle diameter distributions estimated by dynamic light scattering method of CdSe-MPA dispersed aqueous (pH = 6) solution without (black) and with 0.48 nM (red), 0.8 nM (blue), 12 nM (orange) Pt-PVP colloid or 0.5 M (green) ascorbic acid. The particle concentration of CdSe-MPA was 4.0 μM.

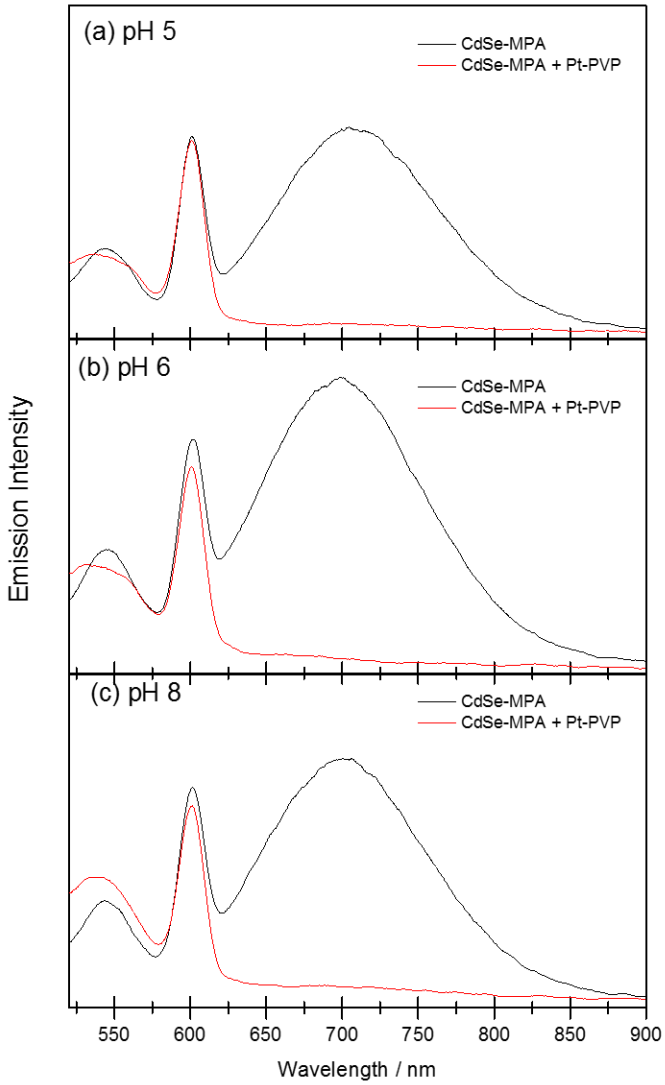

Figure 2-13. Changes of emission spectrum of CdSe-MPA (black) in (a) pH = 5, (b) pH = 6, and (c) pH = 8 by addition of 1.2 nM Pt-PVP colloid (red) (λ_{ex} = 500 nm).

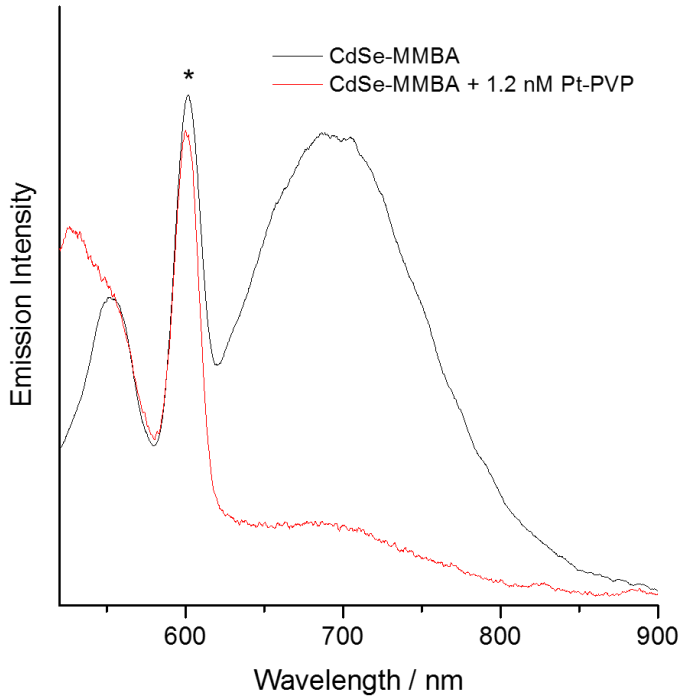

Figure 2-14. Emission spectra of CdSe-MMBA (black), in the presence of Pt-PVP 1.2 nM (red). The peaks indicated by asterisk is Raman scattering of water solvent (λ_{ex} = 500 nm).

2-3-7 Discussion

Considering the above-mentioned results, the dependence of photocatalytic H_2 evolution activity, driven by a CdSe QD as the photosensitizer and a Pt-PVP colloidal catalyst, on the surface passivating ligand is discussed in this section. As mentioned above, the photocatalytic activity for HER increases in the order: CdSe-MMBA < CdSe-4-MBA < CdSe-MPA (Figure 2-8). Among the three CdSe QDs, CdSe-MPA exhibited the best dispersibility in water. Moreover, a broad lower-energy emission originating from the Se-defect site was clearly observed. In the presence of Pt-PVP colloids, CdSe-MPA forms large aggregates (composite of the CdSe QD and Pt colloid) with a diameter of ~1.6 μm [Scheme 2-2(a)]. Moreover, both emissions originate from the band-edge transition state and the Se-defect sites are completely quenched. This suggests that the electron transfer from the CdSe QD to the Pt-PVP colloid occurs effectively via the Se-defect level as shown in Scheme 2-2(c). In contrast, in the case of CdSe-MMBA, comprising ligands with phenyl and methylene groups between the carboxylic acid and thiol groups, large aggregates formed even in the absence of the Pt-PVP colloid [Scheme 2-2

(b)]. This probably occurs because the surface of the CdSe QD is covered by a smaller number of the bulkier MMBA ligands (compared to MPA), resulting in less dispersibility of the CdSe QD in water. These large aggregates are thought to suppress the formation of aggregates with the Pt-PVP colloidal catalyst as suggested by DLS measurements (Table 2-7), implying that the lower efficiency of photoinduced electron transfer from the CdSe QD to Pt-PVP colloidal catalyst than the other two. In the case of CdSe-4-MBA, the Se-defect emission that contributes to the electron transfer from the CdSe QD to the Pt colloidal catalyst was negligible. Furthermore, the photocatalytic HER activity was higher than that of CdSe-MMBA, suggesting that the formation of aggregates composed of a CdSe QD and the Pt-PVP colloid would significantly improve the electron transfer efficiency from the CdSe QD to the Pt-PVP colloid. Thus, the surface passivating ligand plays an important role not only in the stabilization of the CdSe QD, but also in the electron transfer pathway from the photosensitizing CdSe QD to the hydrogen evolving catalyst.

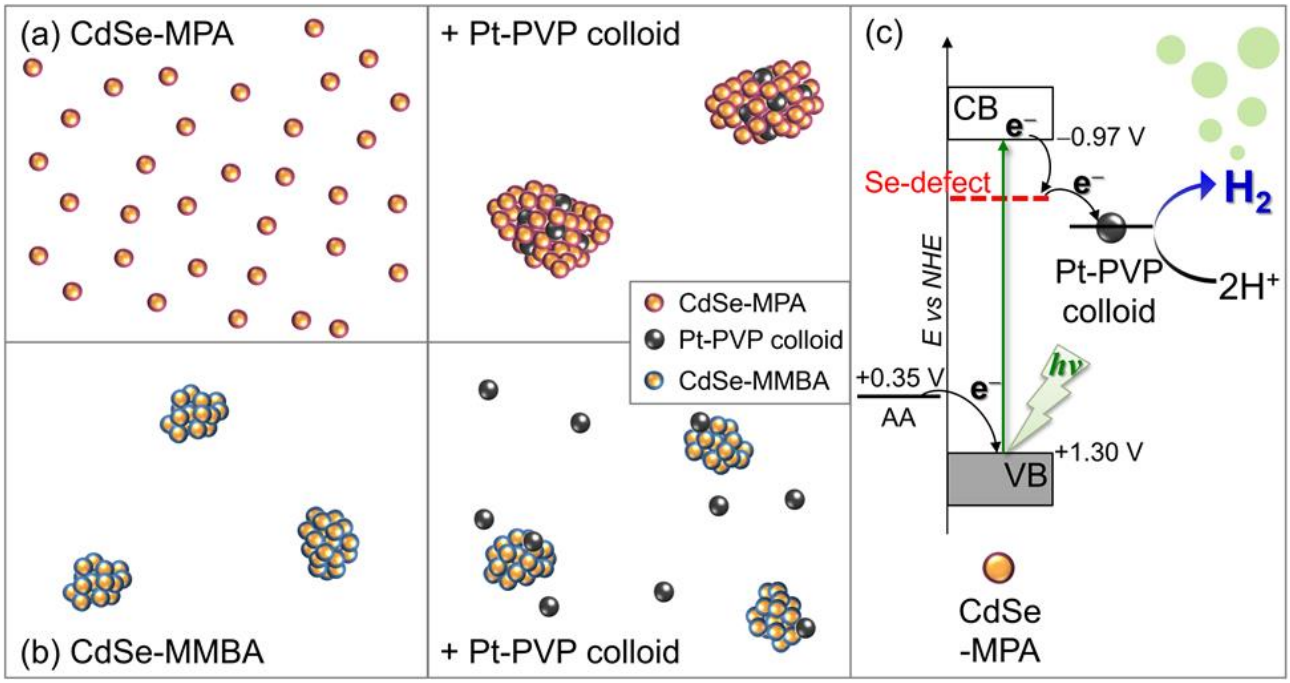

Scheme 2-2. Schematic representations of the aggregates of photosensitizing (a) CdSe-MPA or (b) CdSe-MMBA before (left) and after (right) the addition of the Pt-PVP colloid catalyst. c) Schematic

energy diagram of photocatalytic HER driven by CdSe-MPA and Pt-PVP colloidal catalyst. The values corresponding to the positions of conduction band (CB) minimum, valence band (VB) maximum, and the redox potential of ascorbic acid (AA) are referred from the references[13].

2-4. Conclusion

In this study, a photocatalytic HER driven by photosensitizing CdSe QDs and using PVP-polymer-protected colloidal Pt as the H_2 evolving catalyst has been examined. Although the three CdSe QDs are passivated by similar thiol-based surface passivating ligands (MPA, 4-MBA, or MMBA), they exhibit very different emission behavior. Consequently, CdSe-MPA and CdSe-MMBA exhibit deep trap emissions, probably derived from the surface Se-vacant sites. Conversely, such emissions were negligible in CdSe-4-MBA. This was due to effective hole trapping by the aromatic thiol group. In the presence of a Pt-PVP colloidal catalyst, CdSe-MPA exhibited higher activity for photocatalytic hydrogen production when compared to CdSe-4-MBA and CdSe-MMBA. DLS measurements clearly indicate that the dispersibility of the CdSe QDs in aqueous media is improved in the order: CdSe-MMBA < CdSe-4-MBA < CdSe-MPA, probably due to less steric bulkiness of the surface passivating ligand. In addition, we concluded that the formation of aggregates, composed of CdSe QDs and the Pt colloidal catalyst, plays a crucial role in the photoinduced electron transfer between the photosensitizing CdSe QD and the hydrogen evolving Pt catalyst. Zeta potential measurements indicated that the well-dispersed CdSe-MPA effectively forms aggregates with the Pt colloidal catalyst because of the electrostatic interactions between the negatively charged CdSe QD and the positively charged Pt-PVP colloid. Thus, CdSe-MPA exhibited the highest photocatalytic activity among the three CdSe QDs. The results clearly indicated the importance of the surface passivating ligand; the ligand affects the photophysical properties of CdSe QD as well as the interactions between the photosensitizing CdSe QD and the H_2 evolving catalyst that dominates the photoinduced electron transfer efficiency between them.

References

[1] a) Z.-Q. Yu, X.-M. Xu, C.-Y. Hong, D.-C. Wu, Y.-Z. You, *Macromolecules*, **2014**, *47*, 4136-4143. b) M. C. Schuster, D. A. Mann, T. J. Buchholz, K. M. Johnson, W. D. Thomas, L. L. Kiessling, *Org. Lett.*, **2003**, *5*, 1407-1410.

[2] X. Wang, X. Ren, K. Kahen, M. A. Hahn, M. Rajeswaran, S. Maccagnuno-Zacher, J. Silcox, G. E. Cragg, A. L. Efros, T. D. Krauss, *Nature*, **2009**, *459*, 686-689.

[3] W. W. Yu, L. Qu, W. Guo, X. Peng, *Chem. Mater.*, **2003**, *15*, 2854-2860.

[4] T. Teranishi, M. Hosoe, T. Tanaka, M. Miyake, *J. Phys. Chem. B*, **1999**, *103* 3818-3827.

[5] A. L. Patterson, *Physical Review,* **1939**, *56*, 978-982.

[6] a) Y. Liang, J. E. Thorne, B. A. Parkinson, *Langmuir*, **2012**, *28*, 11072-11077. b) S. F. Wuister, C. de M. Dongená, A. Meijerink, *J. Phys. Chem. B*, **2004**, *108*, 17393-17397.

[7] a) J. Aldana, Y. A. Wang, X. Peng, *J. Am. Chem. Soc.*, **2001**, *123*, 8844-8850. b) I-S. Liu, H.-H. Lo, C.-T. Chien, Y.-Y. Lin, C.-W. Chen, Y.-F. Chen, W.-F. Su, S.-C. Liou, *J. Mater. Chem.*, **2008**, *18*, 675-682.

[8] J. J. Ramsden, M. Grätzel, *J. Chem. Soc. Faraday Trans. 1*, **1984**, *80*, 919-933.

[9] C. F. Landes, M. Braun, M. A. El-Sayed, *J. Phys. Chem. B*, **2001**, *105*, 10554-10558.

[10] a) D. R. Baker, P. V. Kamat, *Langmuir*, **2010**, *26*, 11272-11276.

[11] J. Jasieniak, P. Mulvaney, *J. Am. Chem. Soc.*, **2007**, *129*, 2841-2848.

[12] a) A. Das, Z. Han, M. G. Haghighi, R. Eisenberg, *Proc. Natl. Acad. Sci.*, **2013**, *110*, 16716-16723. b) H. Lv, T. P. A. Ruberu, V. E. Fleischauer, W. W. Brennessel, M. L. Neidig, R. Eisenberg, *J. Am. Chem. Soc.*, **2016**, 138, 11654-11663.

[13] a) J. Huang, K. L. Mulfort, P. Du, L.X. Chen, *J. Am. Chem. Soc.*, **2012**, *134*, 16472-16475. b) L. E. Brus, *J. Chem. Phys.*, **1983**, *79*, 5566-5571. c) L. E. Brus, *J. Chem. Phys.*, **1984**, 80, 4403-4409. d) T. Matsui, Y. Kitagawa, M. Okumura, Y. Shigeta, *J. Phys. Chem. A*, **2015**, *119* 369−376.

Chapter 3

Photocatalytic Hydrogen Evolution Systems using $NiCl_2$

3-1 Introduction

As mentioned in the section of "1-3 Quantum Dot/Rod in Photocatalytic Water Splitting Reaction", several mechanisms of hydrogen evolution reaction in the presence of metal salt as the precursor of the catalyst have been proposed. However, the dominant factors for the formation of the hydrogen evolving catalyst are still unclear.

To investigate the hydrogen evolution mechanism in the presence of the metal salt precursor, three different surface-passivated CdSe QDs, CdSe-MPA, CdSe-3-MBA (3-MBA; 3-mercaptobenzoic acid), and CdSe-4-MBA were selected as the photosensitizer (Scheme 3-1), because the surface condition of CdSe-MPA was significantly different from that of CdSe-4-MBA as discussed in Chapter 2. CdSe-3-MBA was used to clarify the effect of the shape of surface passivating ligand. In this work, $NiCl_2$ was used as the precursor for H_2 evolution catalyst, because two different types of catalysts were reported so far.

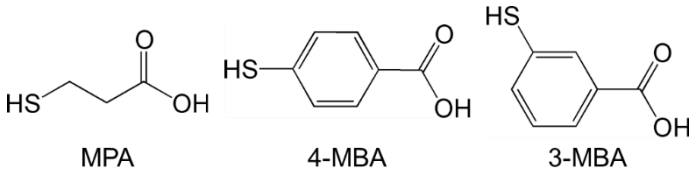

Scheme 3-1. Chemical structures of the surface passivating ligands used in this study: 3-mercaptopropionic acid (MPA), 4-mercaptobenzoic acid (4-MBA), and 3-mercaptobenzoic acid (3-MBA).

3-2 Experimental Section

3-2-1 Material and Methods

Materials.

All commercially available starting materials $[Cd(AcO)_2]nH_2O$, Se, tetradecylphosphonic acid (TDPA), hexadecylamine (HDA), tri-*n*-octylphosphine oxide (TOPO), tri-*n*-octylphosphine (TOP), mercaptopropionic acid (MPA) (Sigma-Aldrich), 3-mercaptobenzoic acid (3-MBA), 4-mercaptobenzoic acid (4-MBA), and 10% tetramethylammonium hydroxide aqueous solution, $NiCl_2 \cdot 6H_2O$ were used as received, and solvents were used without any purification.

Measurements.

UV-Vis absorption and emission spectra were recorded on a Shimadzu MultiSpec-1500 spectrophotometer and a JASCO FP-6600 spectrofluorometer, respectively, using a 1 cm path length quartz cell. Powder X-ray diffraction patterns were recorded on a Bruker D8 Advance diffractometer equipped with a graphite monochromator using Cu-*K*α radiation and a one dimensional LinxEye detector. X-ray Photoelectron Spectroscopy were performed on a JPC-9010MC using Mg Kα excitation. Transmittance electron microscopy was recorded on a JEOL 2010 FASTEM (200kV). The pH of the solutions was controlled by adding sodium hydroxide aqueous solution and dilute hydrochloric acid. Sub-nanosecond pump-probe spectroscopic measurement were performed based on a commercial time-resolved spectrometer (EOS vis-Nir, Ultrafast System).

3-2-2 Synthesis of CdSe-TOPO[1]

The target TOPO-passivated CdSe QD was synthesized according to literature method with minor modification as follows.[2] The mixture of TDPA (0.0755 g), TOPO (4.04 g), and HDA (2.50 g) was put into three-necked flask and dried under vacuum for 30 min at 100 °C. Under N_2 atmosphere,

Se-TOP solution (prepared by dissolving Se (0.079 g) in TOP (1.0 mL)) added to the reaction solution and the mixture was dried again under vacuum at 100 °C for 10 min. After under N_2 atmosphere, Cd-TOP solution (prepared by dissolving $Cd(AcO)_2 \cdot nH_2O$ (0.06 g) in TOP (1.5 mL)) added to the reaction solution at 260 °C and the temperature of reaction solution was downed to 260 °C suddenly, and solution stirred for 4 min at the same temperature. After the 4-min reaction, the temperature of reaction solution decreased quickly to room temperature, and then the solution was diluted with 20 mL of hexane. The emerged colorless precipitates were removed by centrifugation to obtain the target CdSe-TOPO dispersed solution. To purify the solution, 30 mL of MeOH was added to the supernatant solution to form red-precipitates. The precipitates were collected by centrifugation and the almost-colorless supernatant solution was removed. This purification process, i.e. the dispersion in hexane and then precipitation by adding MeOH, was done again. Finally, the precipitate of CdSe-TOPO was dispersed in 2 mL of hexane. The diameter (D) of obtained CdSe QD was estimated by the first excitonic absorption band (λ) observed in UV-vis absorption spectrum using eq. 2-1.[2] The excitonic absorption coefficient per mole (ε) of particles of that was estimated by the diameter from eq. 2-1 using eq. 2-2.[3] The concentration of obtained CdSe QD was estimated by the first excitonic absorption band observed in UV-Vis absorption spectrum using Lambert-Beer's Law (equation 2-3, A: absorbance, C: concentration of QDs particle, L: light path length).

$$D = (1.6122 \times 10^{-9})\lambda^4 - (2.6575 \times 10^{-6})\lambda^3 + (1.6242 \times 10^{-3})\lambda^2 - (0.4277)\lambda + (41.57) \quad \text{equation 3-1}$$

$$\varepsilon = 5857(D)^{2.65} \quad \text{equation 3-2}$$

$$A = \varepsilon CL \quad \text{equation 3-3}$$

3-2-3 Synthesis of thiol covered CdSe QDs[3]

The exchange reaction of the surface passivating TOPO to thiol ligand was performed according to the literature method with minor modification as follows. A mixture of 500 μL hexane

solution of CdSe-TOPO (200 nmol of the nanoparticles) and 8 mL of methanol was put in a two-necked flask and degassed by N_2 bubbling for 5 min. The thiol ligand [3-, 4-MBA (0.3238 g, 2.2 mmol) / MPA (192 μL, 2.2 mmol)] was dissolved in 10% aqueous tetramethylammonium hydroxide solution (1.5 mL of) with methanol (8 mL) in another flask, degassed by N_2 bubbling for 5 min, and then added to the two-necked flask containing the CdSe-TOPO dispersed solution. The mixed solution was refluxed at 65 °C overnight under N_2 atmosphere in dark. After cooling to room temperature, ethyl acetate (20 mL) was added to the reaction solution to emerge red precipitates. Obtained precipitates (CdSe-3,4-MBA / CdSe-MPA) was collected by centrifugation and the supernatant solution was removed. The precipitate was dispersed in H_2O (2 mL) containing two drops of 10% tetramethylammonium hydroxide solution. The concentration of obtained CdSe QD was also estimated by the first excitonic absorption band observed in UV-Vis absorption spectrum using equation 2-1, 2-2 and 2-3.

3-2-4 Photocatalytic hydrogen evolution reaction

Samples were prepared in 40 mL vials and protected from light before use. A 4.0μM $NiCl_2$, 4.0 μM CdSe-QDs (CdSe-4-MBA/ CdSe-3-MBA / CdSe-MPA), and 0.5 M ascorbic acid in H_2O were added to form a total volume of 4.5 mL. The pH of the solutions was adjusted by the addition of aqueous 2 M HCl or 2 M NaOH solution. The samples were sealed with an airtight cap equipped with two rubber septa and then degassed by N_2 bubbling for 1 h. The samples were irradiated from below the vials with OP6-5310HP2 visible light LEDs (λ = 525 nm, Opt-Device Laboratory Ltd). The light power of each LED was set to 40 mW and measured with a COHERENT FieldMaxII-TO laser power meter. During the photoreaction, the samples were stirred using a stirrer tip. The gas in the top-space of the vials was collected using a HAMILTON Microlab 600 auto-dispenser and injected to an Agilent 490 MicroGC gas chromatograph to measure the amount of hydrogen evolved.

3-3 Results and Discussion

3-3-1 Powder X-ray diffraction and transmission electron microscopy

Powder X-ray diffraction patterns of four CdSe QDs are shown in Figure 2-1. All CdSe QDs exhibited very broad but similar diffraction patterns to that of bulk CdSe, indicating that the crystal structures of all four CdSe QDs are the same to the bulk, i.e., the zinc blend structure. Their particle diameters were estimated to be almost constant 2.6 ± 0.2 nm by using Scherrer's equation for broad peak including (100), (002) and (101) reflection. This result indicates that the surface ligand exchange reactions from TOPO to the four different thiols have little effect on the particle size of CdSe QD.

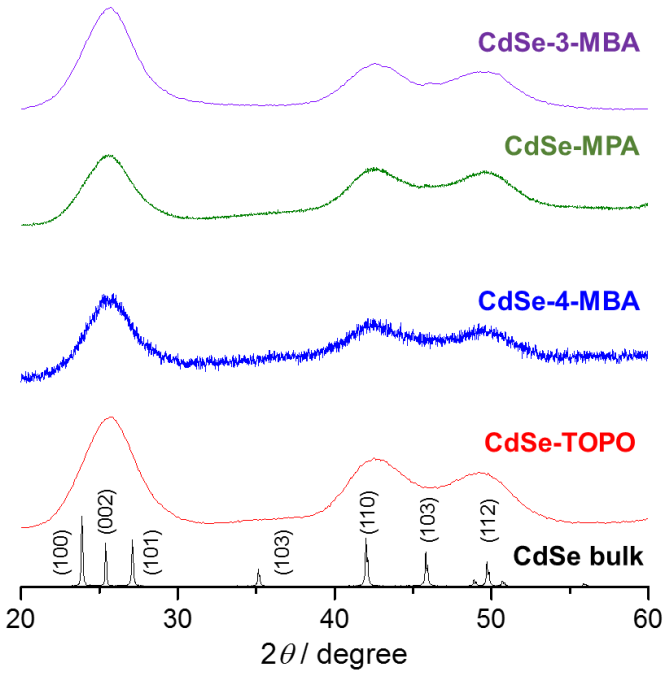

Figure 3-1. Powder X-ray diffraction patterns of bulk CdSe (black), CdSe-TOPO (red), CdSe-4-MBA (blue), CdSe-MPA (green), and CdSe-3-MBA (purple).

3-3-2 UV-vis Absorption and Emission Property

Figure 3-2 shows UV-Vis absorption and emission spectra of the afforded QDs in the dispersed

solution state. The particle size of CdSe QDs can be estimated from the first exciton peak[3]. The CdSe-TOPO, CdSe-*n*-MBA (*n* = 3, 4) and CdSe-MPA QDs exhibited a first exciton peak at almost the same wavelength (listed in Table 3-1), indicating that the particle sizes of these QDs are almost independent of the surface passivating ligand. As discussed in the section of "2-3-2 UV-vis Absorption and Emission Property", the small (compared to that of CdSe-TOPO) red shifts of the first exciton peak observed for thiolate-passivated CdSe QDs are not attributed to the change in particle size but to the differences in the electronic state of the surface ligands. It may be noted that slight but certain difference was observed in the first excitonic peaks between CdSe-3-MBA and CdSe-4-MBA; the peak was observed at slightly blue-shifted by about 1.6 nm for CdSe-3-MBA than that of CdSe-4-MBA. This difference could be due to electronic state of benzene ring and thiol group. The first excitionic absorption band was shifted to lower energy by modifying electro-withdrawing group to benzene ring.[3] In the case of 4-MBA and 3-MBA, they had a different substitution position, which was caused different π conjugation. 3-MBA had carboxyl group and thiol group at meta-position, which was not connected electron conjugation between two groups.

The similar trend was also observed in the emission spectra. CdSe-3-MBA only exhibited negligibly weak emission as well as CdSe-4-MBA. Considering the fact that the thiol group in 3-MBA is directly attached to the phenyl ring, the hole generated by photoirradiation could be delocalized in the whole ligand, resulting in the efficient emission quenching.

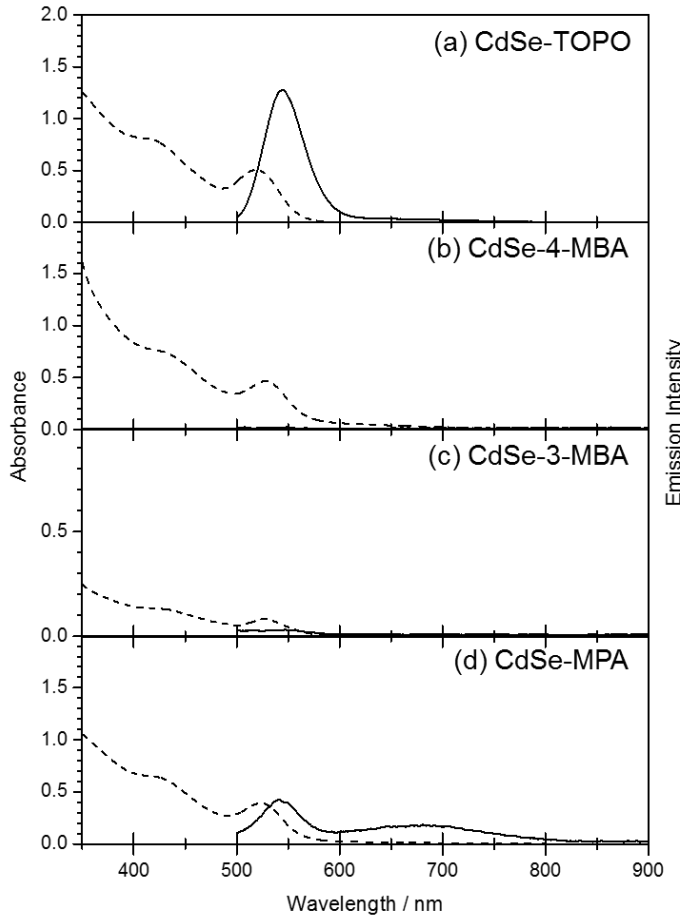

Figure 3-2. UV-Vis absorption (dashed lines) and emission (solid lines) spectra of (a) CdSe-TOPO in *n*-hexane, (b) CdSe-4-MBA, (c) CdSe-3-MBA and (d) CdSe-MPA in basic water; λ_{ex} = 400 nm.

Table 3-1. Absorption and emission peaks for the afforded CdSe QDs.

CdSe QDs	Absorption / nm	Emission / nm
CdSe-TOPO	518.4	543.4
CdSe-4-MBA	528.7	n. d.
CdSe-3-MBA	527.1	n. d.
CdSe-MPA	523.6	541.2, 680.8

3-3-3 X-ray Photoelectron Spectroscopy

As discussed in the previous section, the emission behaviors of two CdSe-*n*-MBA and the other two are significantly different. In order to investigate the origin of the large difference between them, X-ray photoelectron spectroscopic (XPS) measurements were conducted. The results are shown in Figures 3-3 to 3-7. As discussed in the previous chapter, a remarkable difference between CdSe-4-MBA and the other two (CdSe-MPA and CdSe-MMBA) was observed, because of the difference in the electron donating ability of the thiolates. As expected from the similar structures of 3-MBA and 4-MBA, CdSe-3-MBA exhibited very similar XPS spectra to that of CdSe-4-MBA. Observed band widths for Cd 3d peaks for CdSe-3-MBA were also comparable to that of CdSe-4-MBA, suggesting that Se-defect sites were hardly formed in CdSe-3-MBA as well as CdSe-4-MBA. This assumption is consistent to the results of emission spectra shown in Figure 3-2, that is, no emission was observed for both CdSe-*n*-MBA (n = 3, 4).

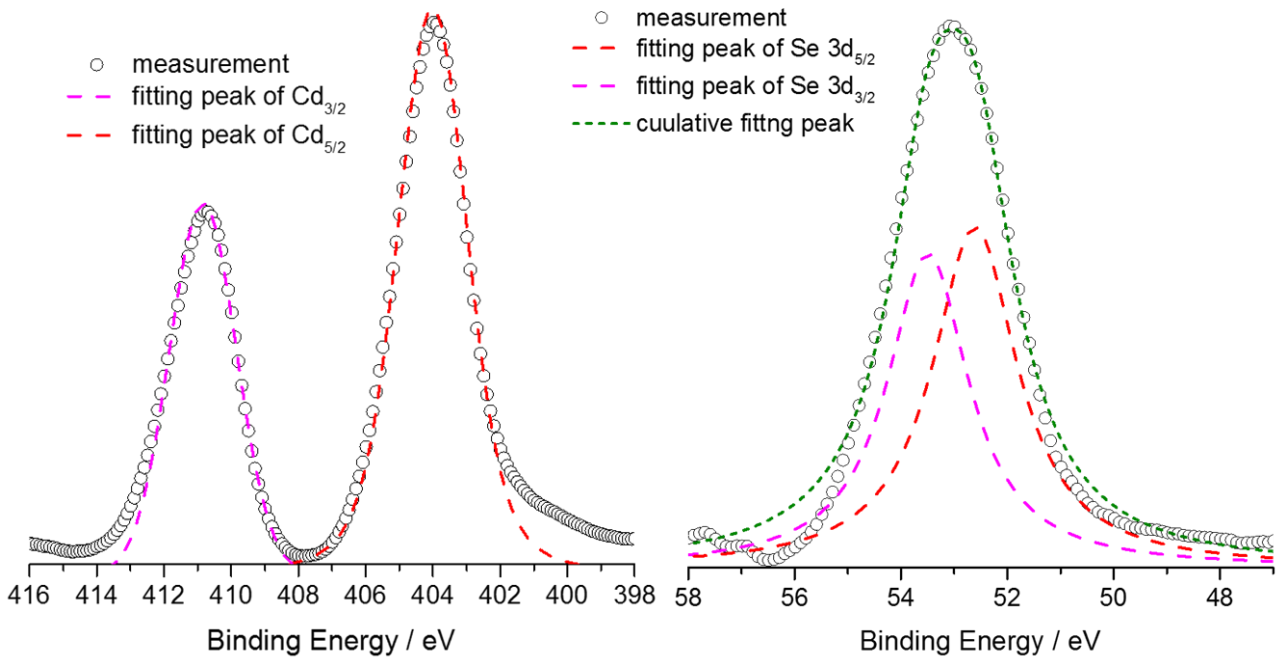

Figure 3-3. XPS spectra of Cd region (left) and Se region (right) of bulk size CdSe.

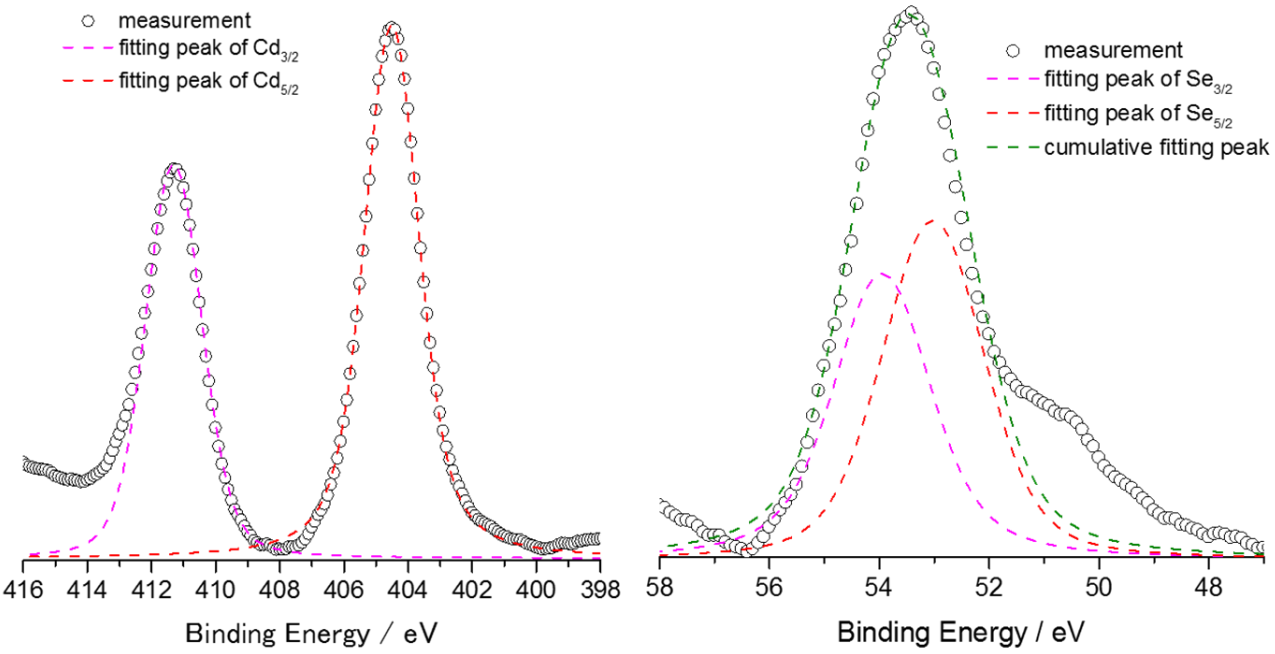

Figure 3-4. XPS spectra of Cd region (left) and Se region (right) of CdSe-TOPO.

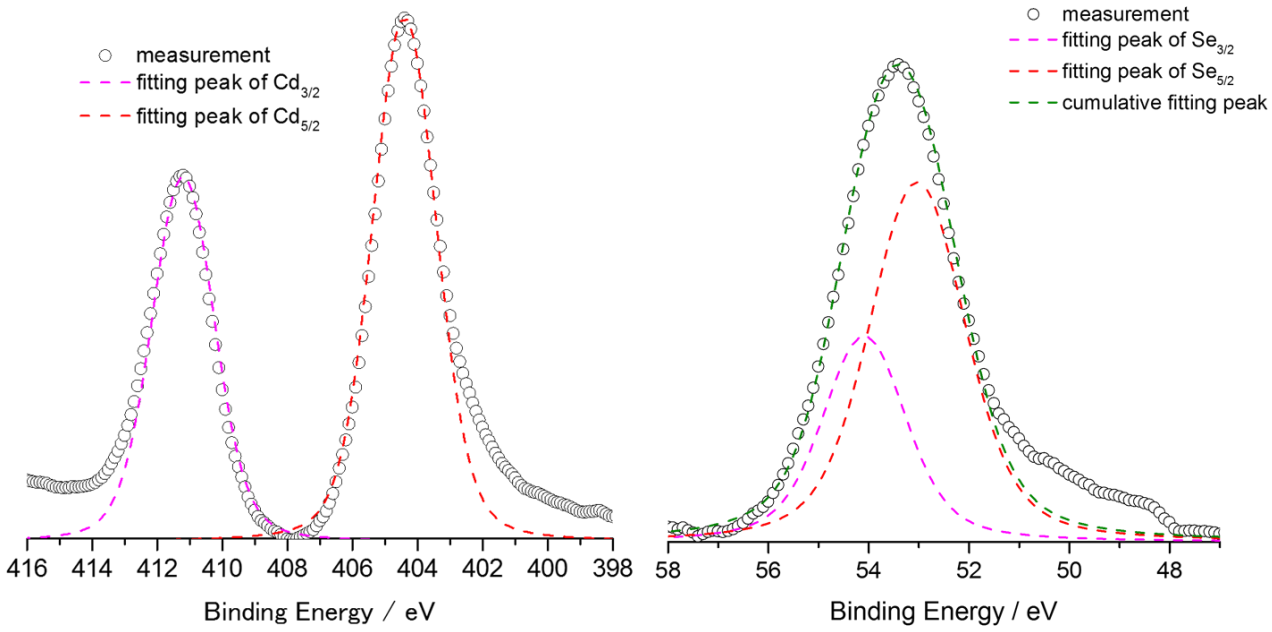

Figure 3-5. XPS spectra of Cd region (left) and Se region (right) of CdSe-4-MBA.

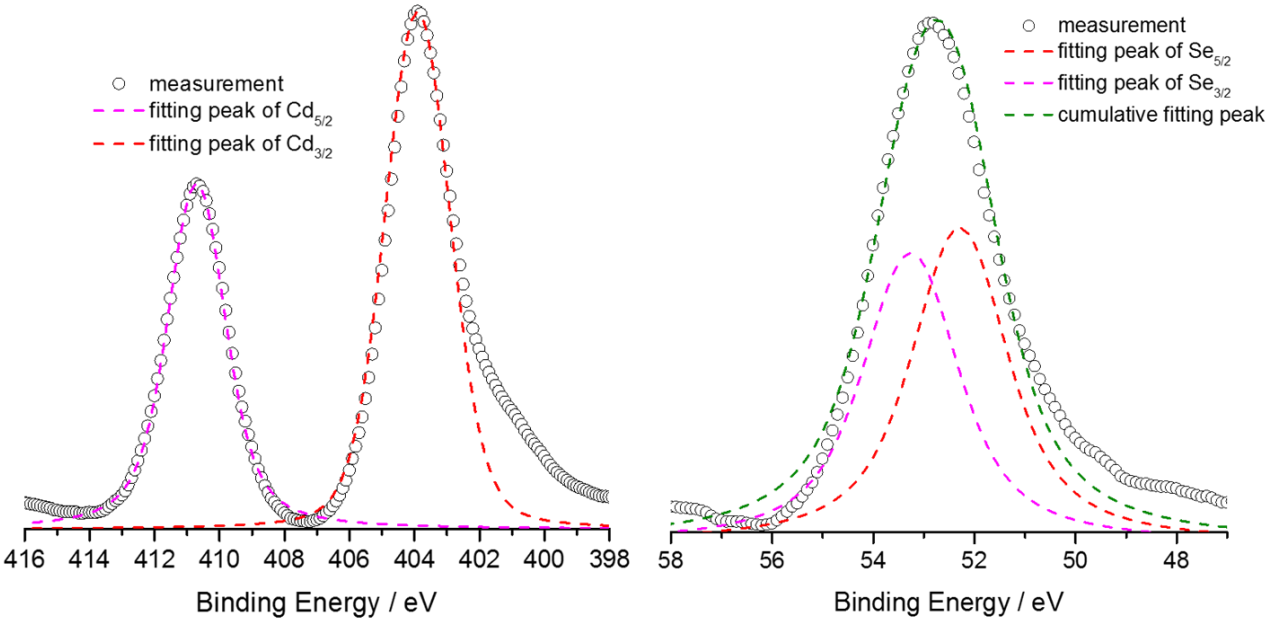

Figure 3-6. XPS spectra of Cd region (left) and Se region (right) of CdSe-3-MBA.

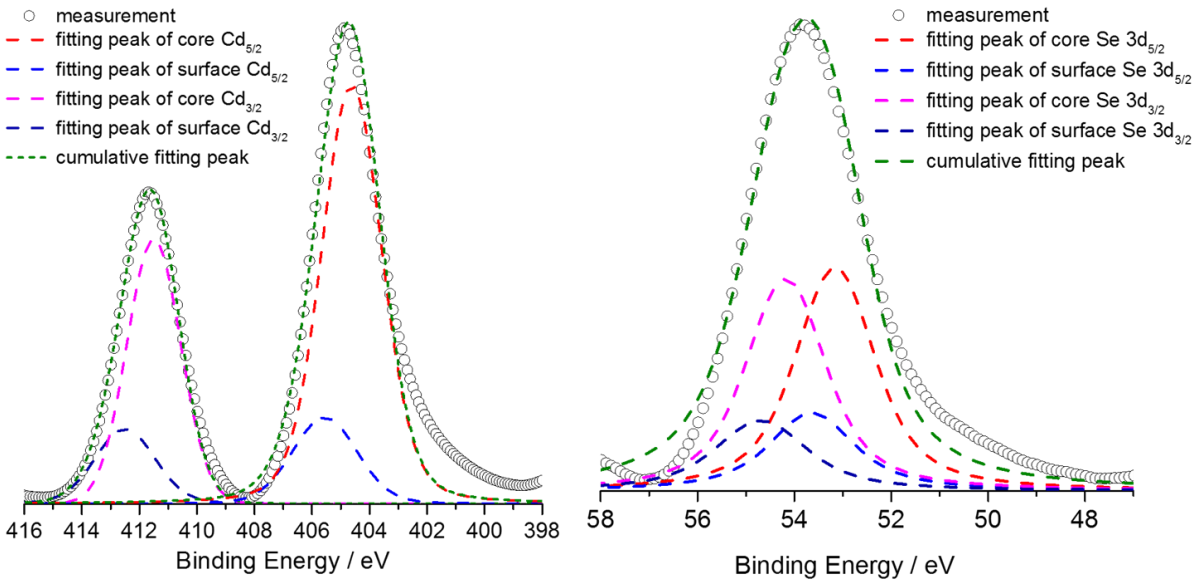

Figure 3-7. XPS spectra of Cd region (left) and Se region (right) of CdSe- MPA.

Table 3-2. Peak-fitting results based on one-component analysis for XPS spectra in Cd 3d region.

Sample	peak		Binding Energy [eV]	FWHM	Area	%Conc.
CdSe (bulk)	Cd 3d 5/2		Peak 1	404.01	2.460	64702.7
	3d 3/2		Peak 1	410.79	2.350	36272.4
CdSe-TOPO	Cd 3d 5/2	Peak 1	404.51	2.039	6773.7	59
	3d 3/2	Peak 1	411.31	2.082	4672.0	41
CdSe-4-MBA	Cd 3d 5/2	Peak 1	404.41	2.330	9052.1	59
	3d 3/2	Peak 1	411.21	2.281	6181.2	41
CdSe-3-MBA	Cd 3d 5/2	Peak 1	403.91	2.380	15115	60
	3d 3/2	Peak 1	410.71	2.134	10115	40
CdSe-MPA	Cd 3d 5/2	Peak 1	404.89	2.654	19997.9	62
	3d 3/2	Peak 1	411.69	2.454	12158.9	38

Table 3-3. Peak-fitting results based on two-component analysis for XPS spectra in Cd 3d region.

Sample	peak		Binding Energy [eV]	FWHM	Area	%Conc.
CdSe-MPA Fitting peaks	Cd 3d 5/2	Peak 1	404.62	2.480	17546.7	53
		Peak 2	405.56	2.664	3745.5	11
	Cd 3d 3/2	Peak 1	411.50	2.205	9098.9	27
		Peak 2	412.50	2.465	3018.3	9
	Se 3d 5/2	Peak 1	53.16	1.965	912.3	37
		Peak 2	53.64	2.102	361.3	15
	Se 3d 3/2	Peak 1	54.18	1.965	867.5	35
		Peak 2	54.69	2.268	343.8	13

Table 3-4. Peak-fitting results based on one-component analysis for XPS spectra in Se 3d region.

Sample	peak		Binding Energy [eV]	FWHM	Area	%Conc.
CdSe (bulk)	Se 3d 5/2		Peak 1	52.61	1.942	920.7
	3d 3/2		Peak 1	53.49	1.862	925.9
CdSe-TOPO	Se 3d 5/2	Peak 1	53.02	2.203	760.1	54
	3d 3/2	Peak 1	53.95	2.105	653.0	46
CdSe-4-MBA	Se 3d 5/2	Peak 1	53.03	2.266	1012.3	66
	3d 3/2	Peak 1	54.09	1.973	515.07	34
CdSe-3-MBA	Se 3d 5/2	Peak 1	52.29	2.268	1471.8	52
	3d 3/2	Peak 1	53.26	2.268	1353.9	48
CdSe-MPA	Se 3d 5/2	Peak 1	53.43	2.679	1435.7	62
	3d 3/2	Peak 1	54.27	2.364	869.4	38

Table 3-5. Peak-fitting results based on one-component analysis for XPS spectra in Se 3d region.

Sample	peak		Binding Energy [eV]	FWHM	Area	%Conc.
CdSe-MPA Fitting peaks	Se 3d 5/2	Peak 1	53.16	1.965	912.3	72
		Peak 2	53.64	2.102	361.3	28
	Se 3d 3/2	Peak 1	54.18	1.965	867.5	72
		Peak 2	54.69	2.268	343.8	28

3-3-4 Photocatalytic hydrogen evolution reaction

Figure 4-1 illustrates the results of the photoinduced hydrogen reaction driven by the photosensitizing CdSe QD and $NiCl_2$ as the precursor of catalyst in aqueous solution (pH = 4). The reaction solution comprise 0.5 M ascorbic acid as the sacrificial electron donor (the wavelength of irradiated light = 525 nm). The determined turnover number (TON) and turnover frequency (TOF) for each solution are summarized in Table 3-6. The TON and TOF values decrease in the order: CdSe-4-MBA > CdSe-MPA > CdSe-3-MBA. It should be noted that this order is completely different to that of the reaction driven by Pt-PVP colloidal catalyst (the order was CdSe-MPA > CdSe-4-MBA, see the section 2-3-4). In addition, no induction period was observed for CdSe-MPA whereas the short induction period about 30 min were observed for two CdSe-*n*-MBA. These results imply that the added $NiCl_2$ precursor would transform the active catalysts which strongly depends on the surface passivating

ligand.

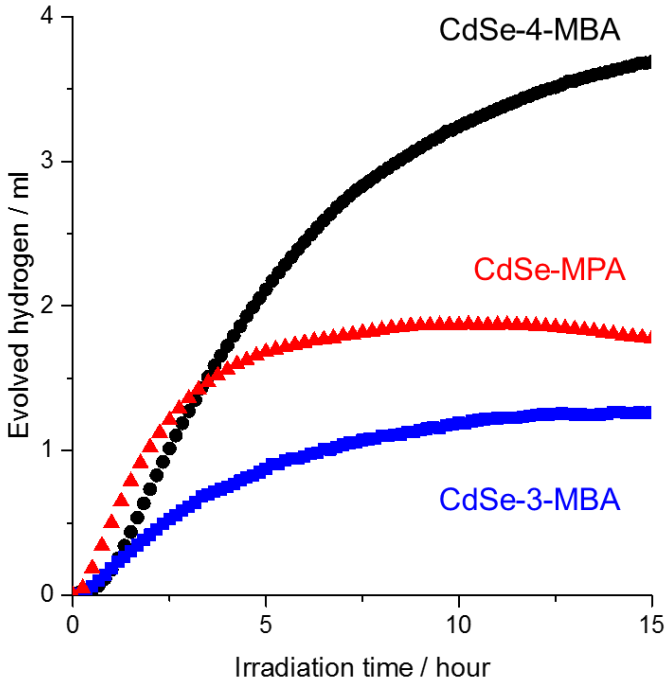

Figure 3-8. Photocatalytic hydrogen evolution reactions (HERs) from aqueous solution (pH 4) comprising 4 μM CdSe-4-MBA (black circles), CdSe-MPA (red triangles), CdSe-3-MBA (blue squares) as the photosensitizer, ascorbic acid (0.5M) as the sacrificial electron donor, and $NiCl_2$ (4 μM) as precursor of hydrogen evolution catalyst; light irradiation at 525 nm.

Table 3-6. Turnover numbers (TON) and maximum turnover frequencies (maxTOF) of photocatalystic hydrogen evolution reaction (HERs) driven by photosensitizing CdSe-QDs and $NiCl_2$.

CdSe-QD	TON[a]	maxTOF
CdSe-MPA	3600	1000
CdSe-4-MBA	7400	1200
CdSe-3-MBA	2500	370

[a.] Turn over numbers per amount of CdSe QD nanoparticles calculated from the amount of hydrogen evolved after irradiation for 15 h.

3-3-5 Transient Absorption Spectroscopy

To understand the electron path form CdSe QDs to Ni species, transient absorption spectra were measured about CdSe-MPA, CdSe-4-MBA and CdSe-3-MBA with and without $NiCl_2$. The result of kinetic trace of transient bleach of the first excitonic absorption of CdSe-MPA, CdSe-4-MBA and CdSe-3-MBA were illustrated from Figure 3-9 to 3-16, respectively. These data were analyzed by the following stretched exponential function and gauss function (eq. 3-4).

$$y = \{\alpha \times \exp[-(t/\tau)^{\beta}] + c \times \exp(-t/u) + d \times exp(-t/v)\} \times \exp[-(x-f)^2/2g^2] \quad \text{eq. 3-4}$$

The former formula is stretched exponential function, which showed electron condition in CdSe QDs and electron path from CdSe QDs to Ni species. In stretched exponential α, c, d denote the scale factor of bleaching, β denote electron distribution in the system, τ, u, v denote the lifetime of bleaching. The latter formula is gauss function, which included instrumental function. In gauss function, f denote correction value of zero time, g denote the factor decided width of gauss function, which included instrumental function. Figure 3-12, 3-13 and 3-14 displayed fitting results for CdSe-MPA, CdSe-4-MBA and CdSe-3-MBA with and without $NiCl_2$. Obtained parameters by fitting based on eq. 3-4 were listed in Table 3-7. Since the long lifetime component over 5 μs estimated from the term c do not affect the electron transfer from CdSe QDs to *in-situ* generated Ni species because manly excited state had short lifetime to ignore diffusion-limited access. β and τ that corresponds to the shorter lifetime component are discussed in detail in this section.

In the case of CdSe-MPA, β values are in the range about 0.6, which means the system is trapping model. The trapping model describes the recombination of excitons in semiconductors.[4] On the other hand, estimated β value for CdSe-MPA are significantly smaller than the others to be about 0.35 in both with and without $NiCl_2$, which means the system is random walk.

Table 3-7. Analysis results based on stretched exponential fitting for kinetic traces of TA spectroscopy about only CdSe QD.

Sample	α	β	τ / ns	c	u / ns	d	f
CdSe-MPA	−0.06573	0.61811	11.75±1.10	−0.00597	394.13	0.06772	0
CdSe-4-MBA	−0.03185	0.47634871	18.84±3.98	−0.00221	14.12	0.03063	−1.13327
CdSe-3-MBA	−0.03024	0.39875	4.31±1.13	−0.00054	9032.79	0.02969	−0.00401

Table 3-8. Analysis result based on stretched exponential fitting for kinetic trace of transient analysis spectroscopy about CdSe QD and $NiCl_2$.

Sample	α	β	τ / ns	c	u / ns	d	f
CdSe-MPA	−0.05508	0.66947	11.88±1.79	−0.00501	481.20	0.05870	0.081
CdSe-4-MBA	−0.03311	0.4861	22.66±3.98	−0.00397	9646.99	0.03307	0
CdSe-3-MBA	−0.02027	0.6307	11.64±2.12	−0.000394	287.62	0.01733	0

Estimated lifetimes (τ) for CdSe-MPA, CdSe-4-MBA and CdSe-3-MBA were 11.75 ns, 18.84 ns and 4.31 ns, respectively. In the absence of $NiCl_2$, the lifetime of CdSe-MPA estimated from the bleaching corresponds to the lifetime estimated from lifetime of fluorescence (2.5 ns).[5] In case of CdSe-4-MBA, emission were not observed (Figure 3-2) because of the complete quenching by hole transfer to the surface-passivating MBA ligand as discussed in the 2-3-2 and 3-3-2 sections. Thus, the more longer lifetime of CdSe-4-MBA than CdSe-MPA is probably due to the charge separated state between the CdSe QD and the surface passivating 4-MBA ligand. From the view point of hole delocalization to the MBA ligand, the lifetime of CdSe-3-MBA is expected to be comparable to that of CdSe-4-MBA. However, the estimated value for CdSe-3-MBA was one-tenth smaller than that of CdSe-4-MBA. It was reported that excited electron of QD could be delocalized in highly energy level CB by spreading LUMO energy level of surface passivating ligands. Thus, longer lifetime of CdSe-4-

MBA was occurred by delocalization of excited electron. However, 3-MBA was differ the position of carboxyl group and thiol group. It affected the rate of delocalization of excited electron, thus CdSe-3-MBA had shorter lifetime than other CdSe QDs. As a result, the hole transfer from CdSe QD to the MBA ligand would be less efficient to 3-MBA than 4-MBA.

After addition of Ni^{2+} ion, lifetime of CdSe-*n*-MBA became longer than without Ni^{2+} ion. However, CdSe-MPA was not affected by addition of Ni^{2+}. These results suggested Ni^{2+} ion affected only aromatic thiol passivating CdSe QDs. In addition, in case of CdSe-*n*-MBA, Ni^{2+} species stood close with CdSe QDs. It is very important for photocatalytic hydrogen evolution reaction, but detail is still unclear.

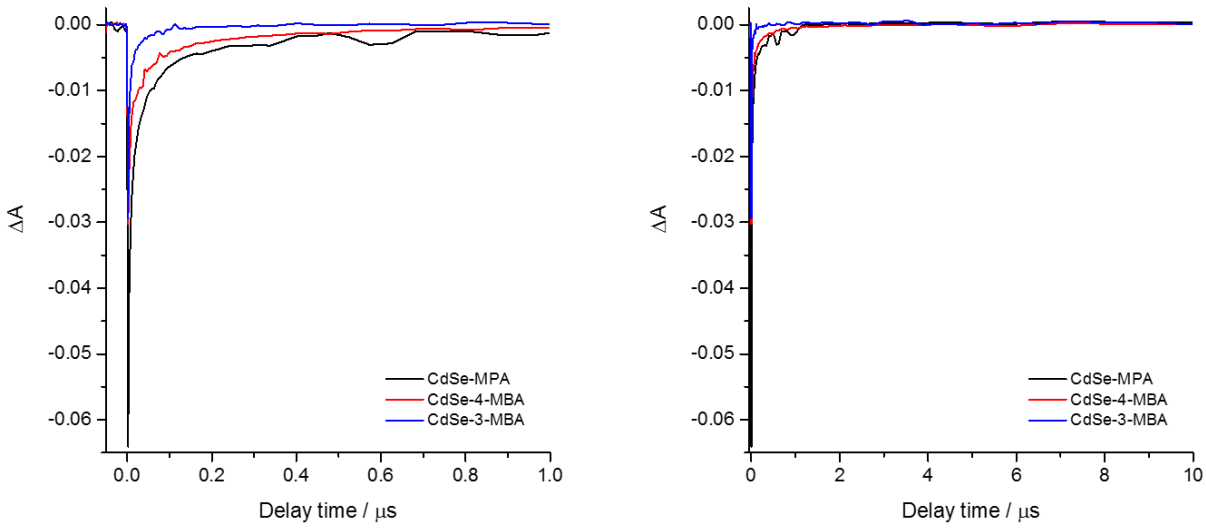

Figure 3-9. Kinetic trace of transient bleach about CdSe-MPA (black), CdSe-4-MBA (red), CdSe-3-MBA (blue) in (left) short temporal window and (right) long temporal window.

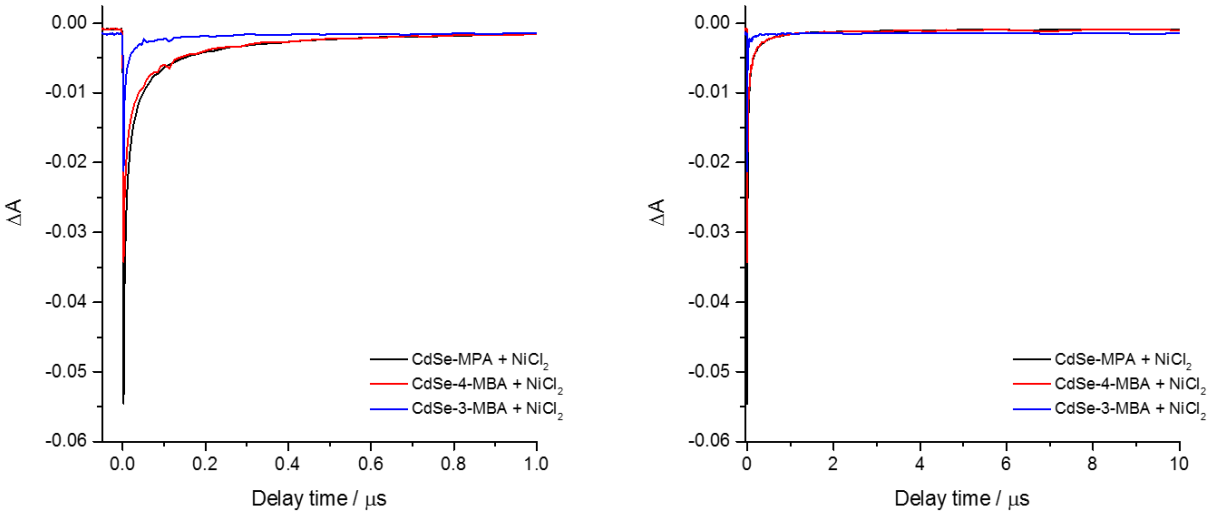

Figure 3-10. Kinetic trace of transient bleach about CdSe-MPA and $NiCl_2$ (black), CdSe-4-MBA and $NiCl_2$ (red), CdSe-3-MBA and $NiCl_2$ (blue) in (left) short temporal window and (right) long temporal window.

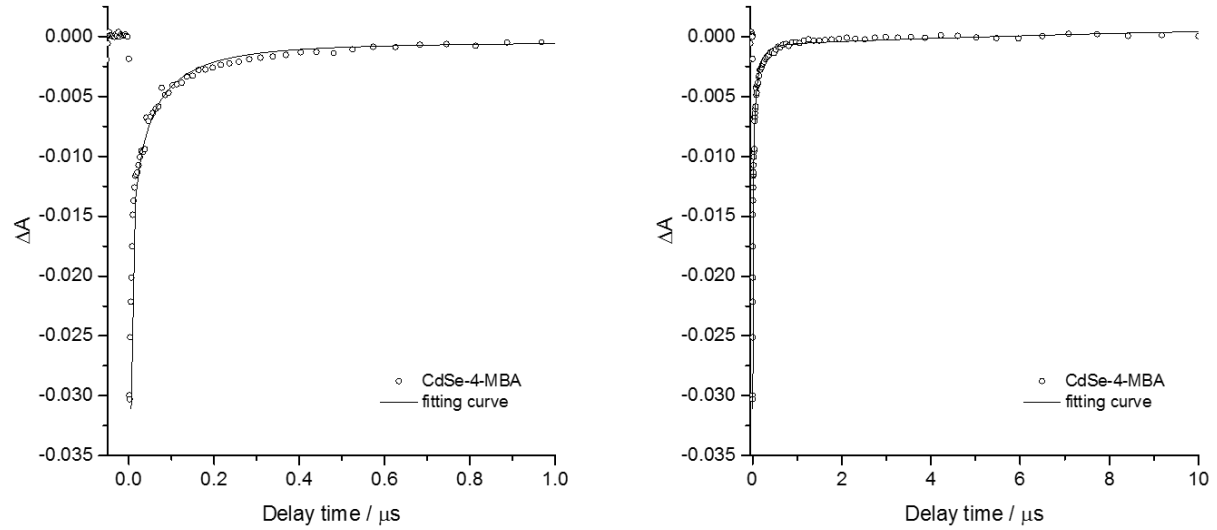

Figure 3-11. Analysis of kinetic trace of transient bleach about CdSe-MPA in (left) short temporal window and (right) long temporal window. Circle: measured date, line: the result of analysis.

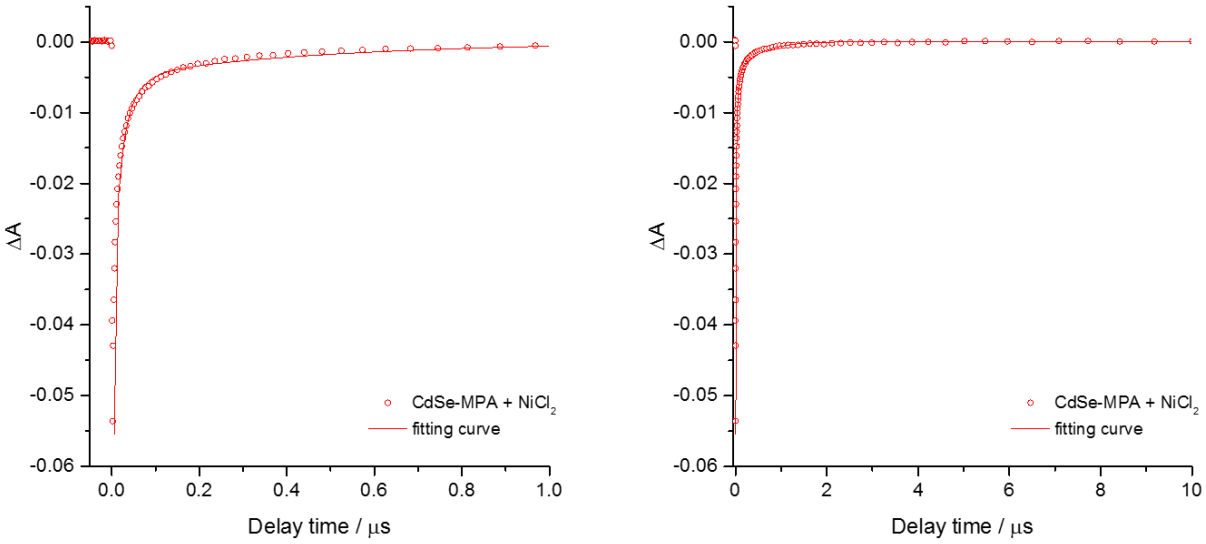

Figure 3-12. Analysis of kinetic trace of transient bleach about the mixture of CdSe-MPA and $NiCl_2$ in (left) short temporal window and (right) long temporal window. Circle: measured date, line: the result of analysis.

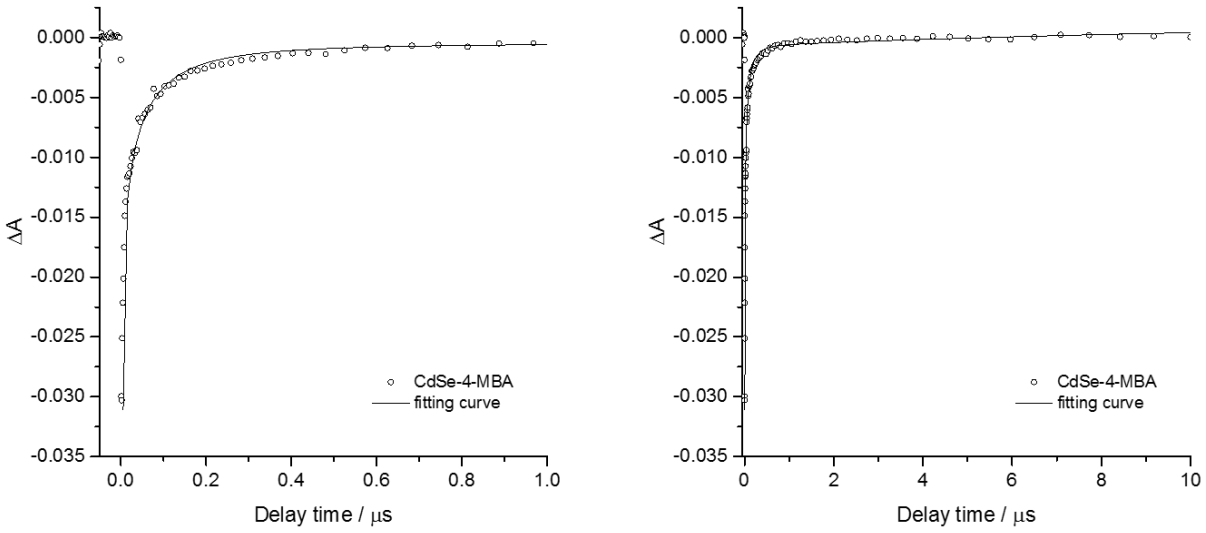

Figure 3-13. Analysis of kinetic trace of transient bleach about CdSe-4-MBA in (left) short temporal window and (right) long temporal window. Circle: measured date, line: the result of analysis.

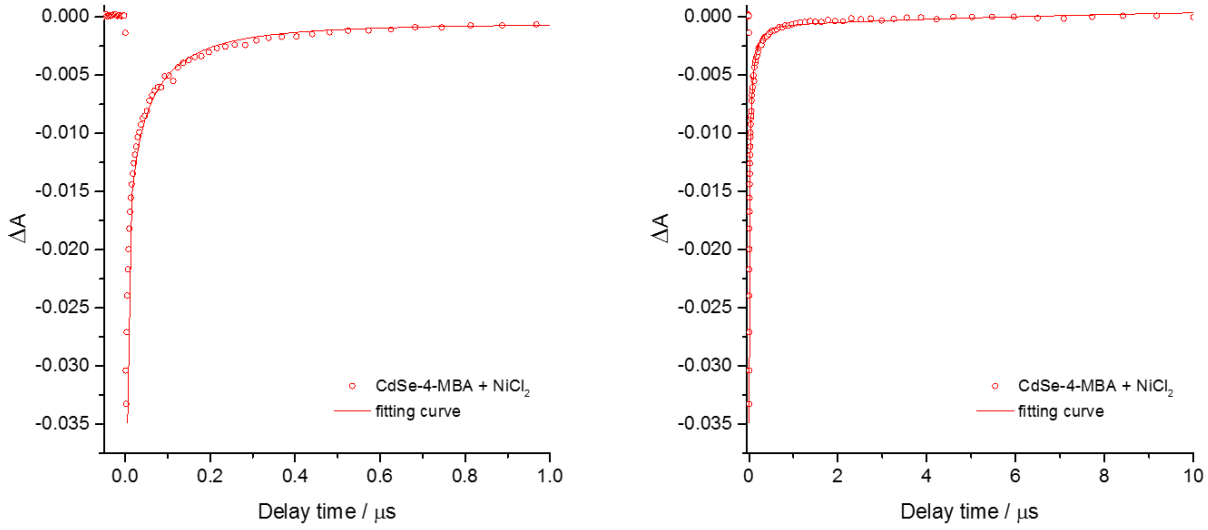

Figure 3-14. Analysis of kinetic trace of transient bleach about the mixture of CdSe-4-MBA and $NiCl_2$ in (left) short temporal window and (right) long temporal window. Circle: measured date, line: the result of analysis.

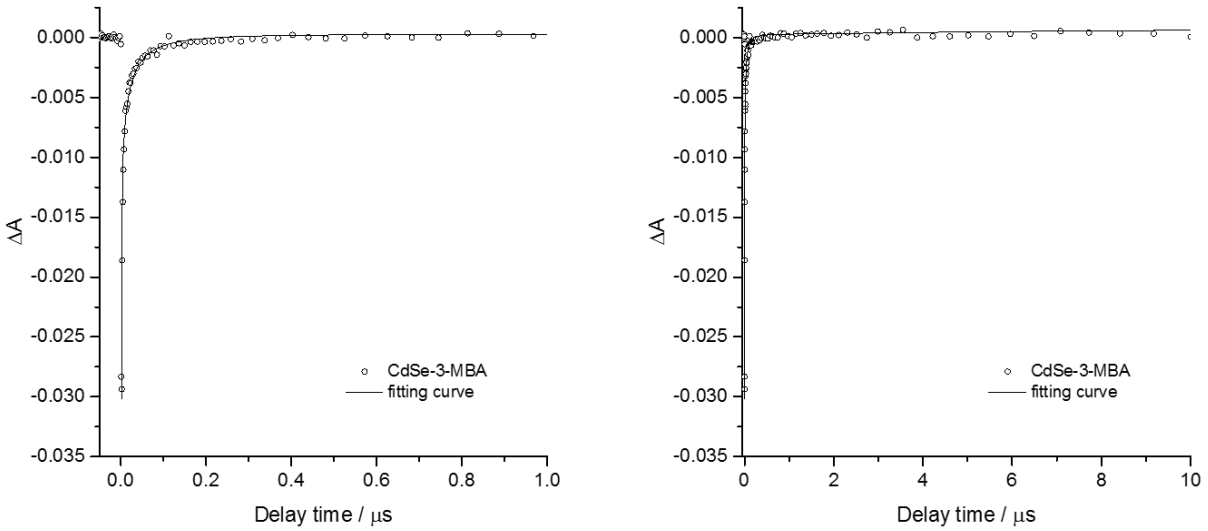

Figure 3-15. Analysis of kinetic trace of transient bleach about CdSe-3-MBA in (left) short temporal window and (right) long temporal window. Circle: measured date, line: the result of analysis.

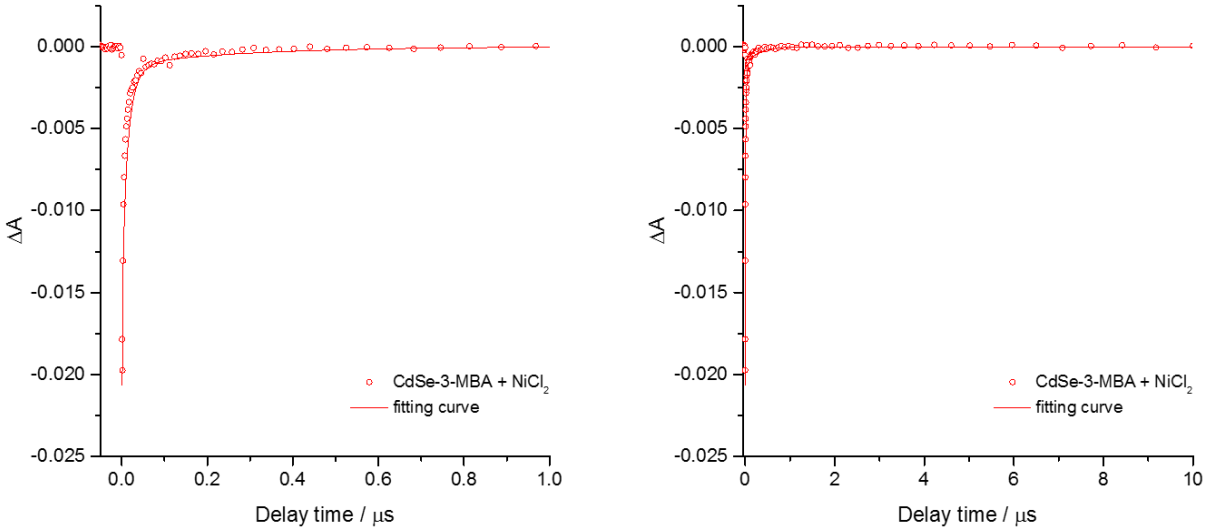

Figure 3-16. Analysis of kinetic trace of transient bleach about the mixture of CdSe-4-MBA and $NiCl_2$ in (left) short temporal window and (right) long temporal window. Circle: measured date, line: the result of analysis.

3-3-6 Cyclic Voltammogram

According to the report by Bernhard *et al*, thiolate-bound Ni(II) complex could be active catalyst for hydrogen evolution reaction.[6] To estimate the catalytic activities of Ni^{2+}-MPA and Ni^{2+}-MBA complex species in the HER, cyclic voltammetry was conducted. Solutions containing $NiCl_2$ (0.25 mM) and MPA or *n*-MBA (2.5 mM) were used for the measurement. As shown in Figure 3-17, the solution containing $NiCl_2$ and MPA showed a large reduction wave below -0.96 V, possibly due to an electrochemical HER. A similar reduction wave was also observed for both solutions containing 4-MBA and 3-MBA, but the potentials were shifted to be negative side by about 0.10 V and 0.12 V than that of $NiCl_2$ with MPA. Considering that the solution without these surface passivating ligands (only $NiCl_2$) shows a very small reduction wave in the same potential region, the *in-situ* generated Ni-thiolate (Ni^{2+}-MPA and Ni^{2+}-*n*-MBA) species could be catalytically active for hydrogen evolution reaction. Judging from the potentials for HER, the activity of *in-situ* generated Ni-MPA species could be more active in than that for the Ni-*n*-MBA species.

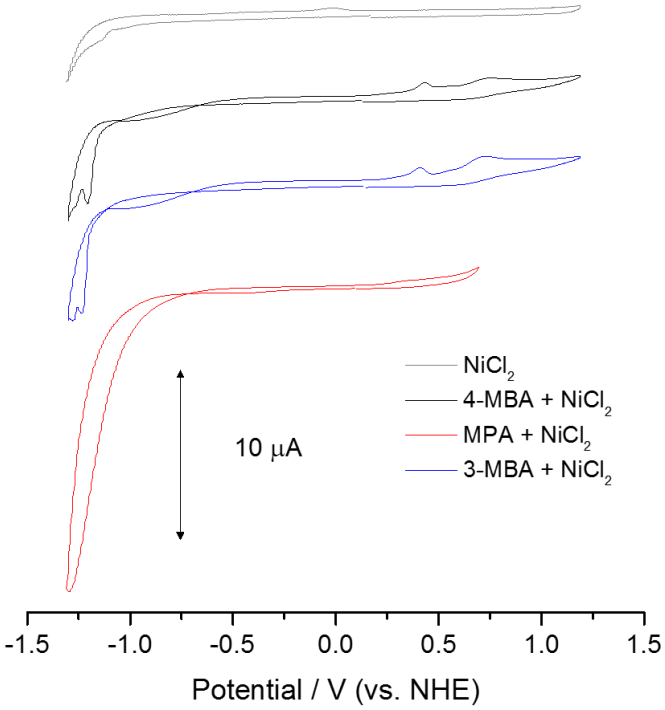

Figure 3-17. Cyclic voltammogram of $NiCl_2$ (gray), the mixture of $NiCl_2$:4-MBA = 1:10 (black), $NiCl_2$: MPA = 1:10 (red), $NiCl_2$: 3-MBA= 1:10 (blue).

3-4 Discussion about photocatalytic HER

Considering the above-mentioned results, the dependence of photocatalytic H_2 evolution activity, driven by a CdSe QD as the photosensitizer and $NiCl_2$ as precursor of hydrogen evolution catalyst, on the surface passivating ligand is discussed in this section. As mentioned above, the photocatalytic activity for HER increases in the order: CdSe-3-MBA < CdSe-MPA < CdSe-4-MBA (Figure 3-8). Nevertheless, the *in-situ* generated Ni-MPA complex species could be more active in electrochemical HER than that for the Ni-MBA species, as seen in Figure 3-17. The reason for this inconsistency could also be due to the surface Se-vacant sites of CdSe-MPA, as shown in emission spectra (Figure 3-2) and XPS measurement (Figure 3-7). It was caused by the strong bonding between surface Cd and thiol atom of MPA. Thus, CdSe-MPA was hardly to release the surface passivating ligand, MPA. On the other hand, CdSe-*n*-MBA was easy to release the surface passivating ligand, *n*-MBA because Cd-S bond between surface Cd and thiol atom of *n*-MBA was not so strong. If there are free surface passivating ligand in the reaction solution in every CdSe QDs, the order of HER have agreed the order of electrochemical HER. Thus, there are some mechanism about hydrogen evolution reaction used $NiCl_2$ as precursor. CdSe-MPA could trap Ni^{2+} and trapped Ni would act as the hydrogen evolution catalyst.[7] Thus, in this system CdSe-MPA would evolve hydrogen after trapping Ni^{2+}. However, CdSe-*n*-MBA did not have the surface defect and it was easy to release *n*-MBA. Thus, system of CdSe-*n*-MBA would evolve hydrogen after coordination with Ni^{2+}.

From transient absorption measurement, lifetime of CdSe-3-MBA was shorter than that of CdSe-4-MBA. It affected the activity of HER, thus the lowest HER activity was observed in the system of CdSe-3-MBA. In case of CdSe-MPA, the catalyst was trapped at the surface of CdSe QDs. Despite of short lifetime, this distance was enough to transfer electron from CdSe-MPA to Ni catalyst. However, it was not enough to transfer electron from CdSe-3-MBA to Ni-3-MBA because CdSe-3-MBA was molecular catalyst. In the system of CdSe-4-MBA, the active species was also molecular catalyst. However, it was easy to transfer from CdSe-4-MBA to Ni species because the lifetime was long.

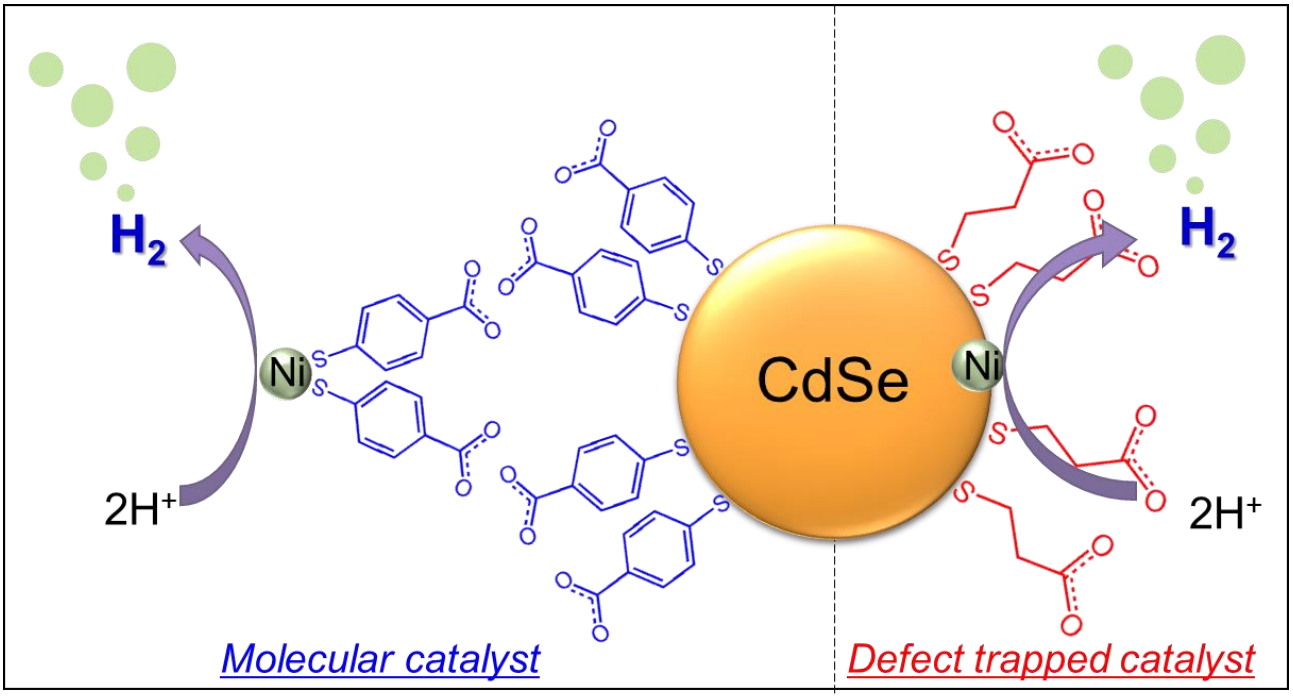

Scheme 3-2. Schematic representations of Ni catalytic hydrogen evolution reaction in the system of CdSe-4-MBA (left) or CdSe-MPA (right).

3-5 Conclusion

In this study, a photocatalytic HER driven by photosensitizing CdSe QDs and using $NiCl_2$ as precursor of the H_2 evolving catalyst has been examined. Although the three CdSe QDs are passivated by similar thiol-based surface passivating ligands (MPA, 4-MBA, or 3-MBA), they exhibited very different emission behavior; CdSe-MPA exhibited deeply trapped emissions derived from the surface Se-vacant sites. Conversely, such emissions were negligible in CdSe-*n*-MBA. This was due to effective hole trapping by the thiol group directly attached on the electron accepting phenyl ring. In the presence of $NiCl_2$, the TON for photocatalytic hydrogen production is found to be highest for CdSe-4-MBA and followed by CdSe-MPA and CdSe-3-MBA. Cyclic voltammogram revealed that the electrochemical HER activity of Ni(II) complexes composed of the surface passivating ligands improved in the order: 3-MBA < 4-MBA < MPA. This disagreement between the photocatalytic and electrocatalytic activities is thought to be the difference of the HER catalyst. The tight Cd-S bonding of MPA not only prevent CdSe-MPA from forming the catalytically active Ni(II)-MPA species, but also promote the formation of catalytically active Ni sites on the surface of CdSe QD. In contrast, the relatively weaker Cd-S bonds of CdSe-*n*-MBA enable them to generate *in-situ* Ni-MBA molecular catalyst. These results clearly indicate the importance of surface passivating ligand in the photocatalytic HER and also suggest that the molecular structure and electron donating ability of the thiolate-based surface passivating ligand directly affected the mechanism of photocatalytic HER.

Reference

[1] X. Wang, X. Ren, K. Kahen, M. A. Hahn, M. Rajeswaran, S. Maccagnuno-Zacher, J. Silcox, G. E. Cragg, A. L. Efros, T. D. Krauss, *Nature*, **2009**, *459* 686-689.

[2] W. W. Yu, L. Qu, W. Guo, X. Peng, *Chem. Mater.*, **2003**, *15*, 2854-2860.

[3] M. B. Teunis, S. Dolai, R. Sardar,, *Langmuir*, **2014**, *30*, 7851−7858

[4] J. C. Phillips, *Rep. Prog. Phys.*, **1996**, *59*, 1133-1207.

[5] D. R. Baker, P. V. Kamat, *Langmuir*, **2010**, *26*, 11272-11276.

[6] H. N. Kagalwala, E. Gottlieb, G. Li, T. Li, R. Jin, S. Bernhard, *Inorg. Chem.*, **2013**, *52*, 9094−9101.

[7] Z.-J. Li, J.-J. Wang, X.-B. Li, X.-B. Fan, Q.-Y. Meng, K. Feng, B. Chen, C.-H. Tung, L.-Z. Wu, *Adv. Mater.*, **2013**, *25*, 6613–6618.

Chapter 4

General conclusion

In this study, to clarify the effect of the surface passivating ligand on CdSe QD to the mechanism of photocatalytic hydrogen evolution reaction, four types of surface passivating ligands (MPA, 4-MBA, 3-MBA, and MMBA) and two types of catalysts, well-known Pt colloidal catalyst and $NiCl_2$ precatalyst, were used and investigated in detail.

In chapter 1, general introduction and remarkable properties noticed in this thesis such as solar water splitting and photocatalyst, photocatalytic hydrogen evolution reaction, photosensitizer, quantum dot, quantum dot in photocatalytic water splitting reaction, were briefly summarized.

In chapter 2, the aggregation between Pt-PVP colloid and CdSe QDs was found to depend strongly on the surface passivating ligand. The molecular volume of surface passivating ligand considerably affect the density of surface passivating ligand on the surface of CdSe QD, resulting in the dispersibility of CdSe QDs to aqueous solution. The key finding in this study is the good correlation between the photocatalytic activity for HER and the dispersibility of CdSe QD; highly and negatively charged CdSe-MPA exhibited best dispersibility in water and highest photocatalytic activity for HER. Thus, in the system containing Pt-colloidal catalyst, the surface passivating ligand plays an important role on the formation of aggregates composed of photosensitizing CdSe QDs and Pt-colloidal catalyst to regulate the photo-induced electron transfer efficiency from CdSe QD to Pt colloid (see Figure5-1).

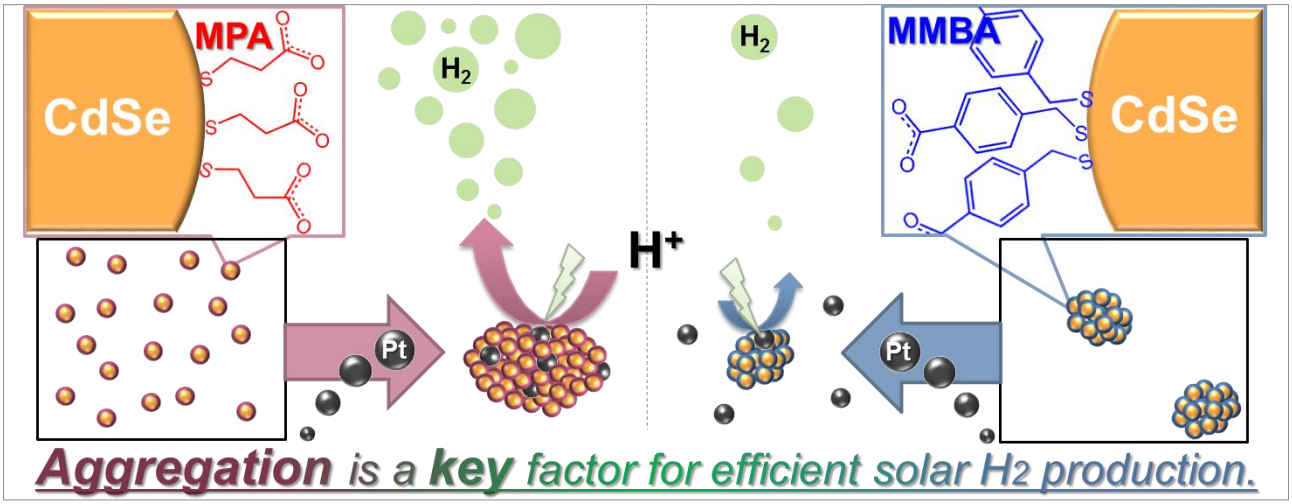

Figure 5-1. Schematic representations of the photocatalytic H_2 evolution driven by the aggregates composed of photosensitizing CdSe-MPA (left) and CdSe-MMBA (right) .

In chapter 3, the mechanism of photocatalytic hydrogen evolution reaction was suggested to depend on the surface passivating ligand. MPA ligand with stronger σ-donating ability coordinated to the surface Cd atom, leading to the formation of Se-vacant surface defect. In the presence of Ni^{2+} ion, Ni^{2+} cations would be trapped at the surface defects to form a catalytically active Ni sites on the surface of CdSe QD (see Figure 5-2(right)). On the other hand, the bonds between n-MBA (n= 3,4) ligands with weaker σ-donating ability than that of MPA and Cd atoms on the surface would not be strong enough to form of Se-vacant site, resulting in the release of MBA ligand from the surface of CdSe QD to form catalytically active molecular Ni-MBA species.

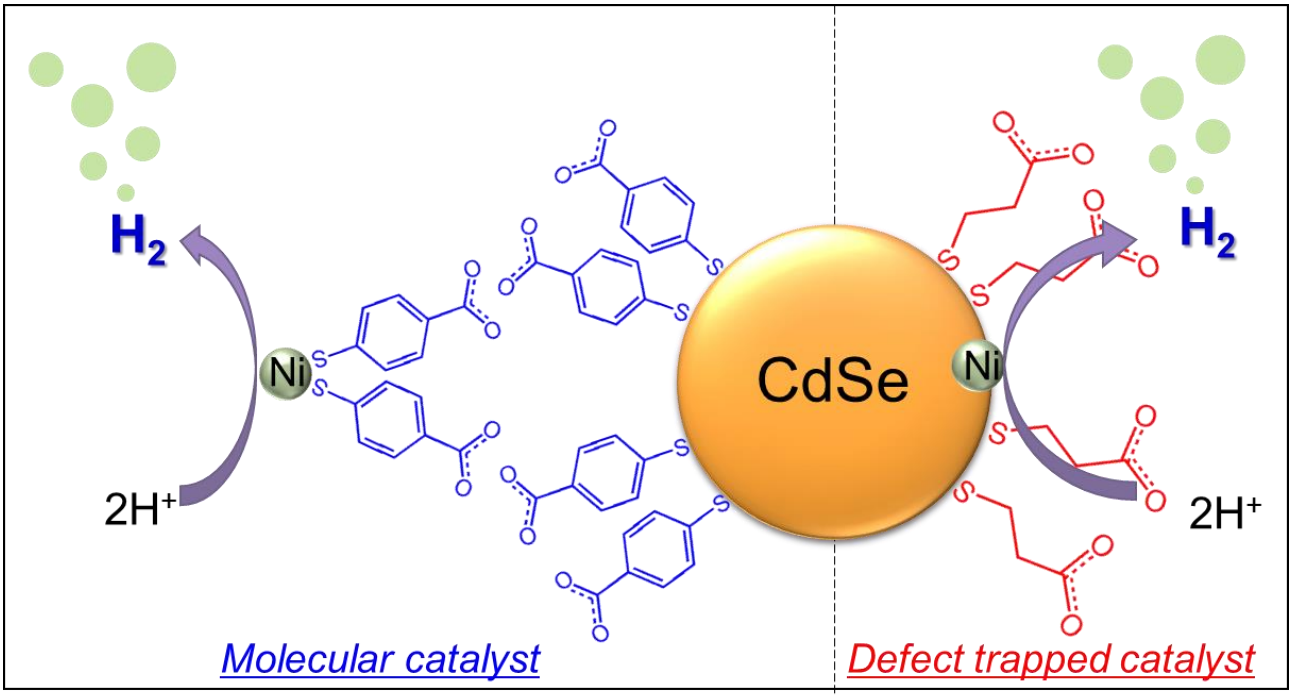

Figure 5-2. Schematic representations for photocatalytic HER of CdSe-4-MBA (left) and CdSe-MPA (right) in the presence of Ni^{2+} ion.

In this thesis, the role of surface passivating ligand of CdSe QD was investigated deeply through consideration of two different hydrogen evolution catalysts. The results obtained in this thesis clearly indicate the importance of the surface passivating ligand; the molecular and electronic structures of surface passivating ligand affected not only the surface condition of CdSe QDs but also the mechanism of hydrogen evolution reaction. This thesis is a new approach to use the surface passivating ligand of nanoparticles.

Acknowledgment

This study on this thesis has been carried out under the direction of Professor Masako Kato during April 2013 – March 2017 at the Materials Chemistry and Engineering course, Graduate School of Chemical Sciences and Engineering, Hokkaido University.

The author is greatly indebted to Professor Msako Kato for her earnest guidance and proper suggestion. The author is deeply grateful to Associate Professor Atsushi Kobayashi for his proper suggestion and earnest encouragement toward not only my research but also my life as a researcher. The author is thankful to Assistant Professor Masaki Yoshida for helpful advice and suggestion thought this work.

Moreover, the author would like to express thank Prof. Noboru Kitamura, Prof. Sadamu Takeda and Prof. Yasuchika Hasegawa (Hokkaido University) for insight full comments and suggestions. The author would like to express thank Prof. Ho-Chol Chang and Assistant Professor Takeshi Matsumoto (Chuo University) for helpful advice and suggestion. The author would like to express my gratitude to Prof. Yasuchika Hasegawa and Dr. Akira Kawashima (Hokkaido University) for their support with transmission electron microscopy measurements. The author would like to express my gratitude to Prof. Hideki Hashimoto, Ms. Nao Yukihira and Mr. Hiroki Sato (Kanseigakuin University) for their support and discussions on transient absorption measurements and analysis.

The author thankful to Ms. Mayu Shimizu, Ms. Mariko Tsukada and Ms. Zeff Yuriko for their secretarial works and warm encouragement. Acknowledgements are all members of the group of Professor Kato for their friendship during the time in the laboratory, especially Mr. Tomohiro Ogawa, Mr. Yasuhiro Shigeta and Mr. Hirotsugu Kitano. The author thankful to colleague in the department of chemistry.

This work was supported by a KAKENHI grant from the JSPS Research fellow (15J05927), and Artificial Photosynthesis (grant no. 2406) from MEXT, Japan.

Finally, the author would also like to express the deepest gratitude to her family, Ms. Nori Naito, Ms. Minako Sawaguchi and Dr. Takuto Sato for the best encouraging sympathizer.

Kana Sato (Sawaguchi)

Graduate School of Chemical Science and Engineering

Hokkaido University

March 2017